J. Fluid Mech. (1994), *vol.* 260, *pp.* 155–184

The current emitted by highly conducting Taylor cones

By J. FERNÁNDEZ DE LA MORA AND I. G. LOSCERTALES
Yale University, Mechanical Engineering Department, New Haven, CT 06520, USA

(Received 16 August 1992 and in revised form 5 July 1993)

When a liquid meniscus held at the exit of a metallic capillary tube is charged to a high voltage V, the free surface often takes the form of a cone whose apex emits a steady microjet, and thus injects a certain charge I and liquid volume Q per unit time into the surrounding gas. This work deals with liquids with relatively large conductivities K, for which the jet diameter d_j is much smaller than the diameter d_n of the capillary tube. In the limit $d_j/d_n \to 0$, the structure of the jet (d_j and I, in particular) becomes independent of electrostatic parameters such as V or the electrode configuration, being governed mostly by the liquid properties and flow rate Q. Furthermore, the measured current is given approximately by $I = f(\epsilon)\,(\gamma QK/\epsilon)^{\frac{1}{2}}$ for a wide variety of liquids and conditions (ϵ, and γ are, respectively, the dielectric constant of the liquid and the coefficient of interfacial tension; $f(\epsilon)$ is shown in figure 11). The following explanation is proposed for this behaviour. Convection associated with the liquid flow Q transports the net surface charge towards the cone tip. This upsets the electrostatic surface charge distribution slightly at distances r from the apex large compared to a certain charge relaxation length λ, but substantially when $r \sim \lambda$. When the fluid motion is modelled as a sink flow, λ is of the order of $r^* = (Q\epsilon\epsilon_0/K)^{\frac{1}{3}}$ (ϵ_0 is the electrical permittivity of vacuum). If, in addition, the surface charge density is described through Taylor's theory, the corresponding surface current convected towards the apex scales as $I_s \sim (\gamma QK/\epsilon)^{\frac{1}{2}}$, as observed for the spray current. The sink flow hypothesis is shown to be realistic for sufficiently small jet Reynolds numbers. In a few photographs of ethylene glycol cone jets, we find the rough scaling $d_j \sim 0.4r^*$ for the jet diameter, which shows that the jet forms as soon as charge relaxation effects set in. In the limit $\epsilon \gg 1$, an upper bound is found for the convected current at the virtual cone apex, which accounts for only one-quarter of the total measured spray current. The rest of the charge must accordingly reach the head of the jet by conduction through the bulk.

1. Introduction

When the interface between a gas and a conducting liquid is charged to a sufficiently high electrical potential, it often takes the form of a stable cone, whose apex emits a microscopic liquid filament (figure 1). Although such remarkable structures have been studied systematically for a long time (Zeleny 1914, 1915, 1917; Taylor 1964, p. 392), very little is known theoretically on the phenomena controlling either the microjet streaming from the cone apex, or the magnitude of the current I it emits. One knows, however, that the radius of this jet may vary in practice from atomic dimensions in liquid metals (Benasayag & Sudraud 1985; Gabovich 1984) up to hundreds of micrometers in liquids with conductivities K in the range of 10^{-7} S m^{-1} (Jones & Thong 1971; Gomez & Tang 1991*a*, *b*, Cloupeau & Prunet-Foch 1989). These jets are far longer and substantially less unstable than their uncharged counterparts, but eventually

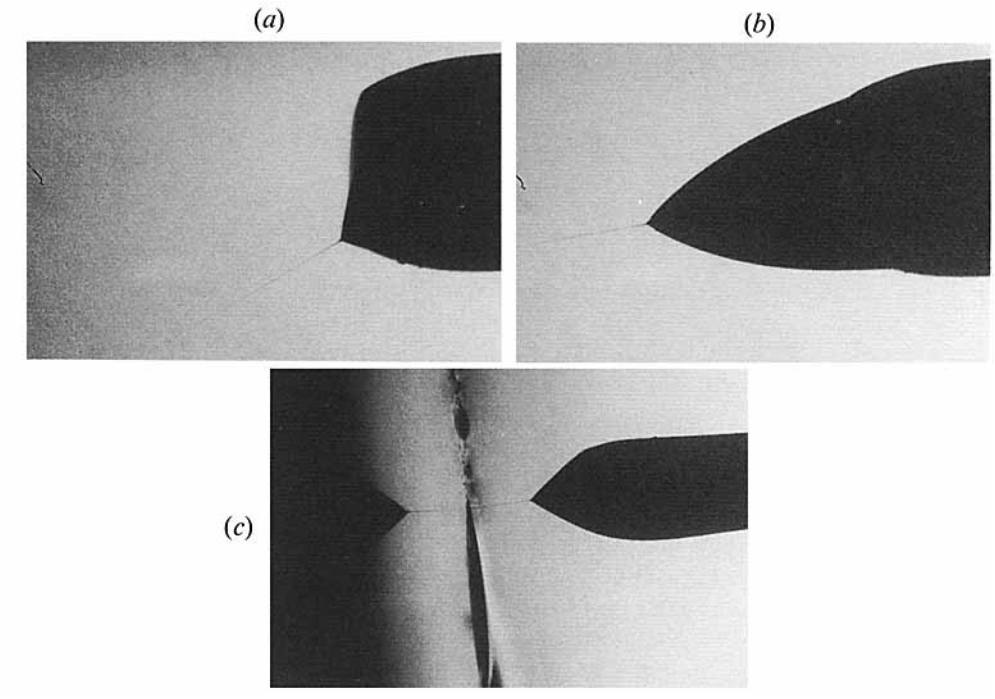

FIGURE 1. Photographs of electrified cones of ethylene glycol (EG-5 in table 2) at various extreme electrostatic conditions within which the emitted current depends only on flow rate and not on voltage difference V, or the distance L between needle and ground. In (*a*) and (*b*) $V = 5$ kV ($I_a = 41.0$ nA) and 3 kV ($I_b = 41.6$ nA), respectively; $L = 9$ mm. In (*c*) the liquid reaches the surface before opening into a spray.

break into a spray (electrospray) of droplets which are often of a single size and may be charged near the maximum value permitted by the Rayleigh instability. Such a singular behaviour has led to numerous studies of the phenomenon and to a wide variety of applications (Bailey 1988). Interest in electrosprays has been recently revitalized by the discovery in 1988 of so-called 'electrospray ionization' as a way of converting solution ions into highly charged gas-phase ions of macromolecules (see the review by Fenn *et al.* 1989). The unusually high charge level in these macro-ions allows their mass analysis in simple quadrupole filters, a circumstance which has literally revolutionized the mass spectrometry of proteins and other large biomolecules (Smith *et al.* 1991 discuss over 300 related references). Consequently, there is now a growing need to understand the fundamental mechanisms behind this phenomenon.

An electrohydrostatic explanation of these pointed menisci was proposed by G. I. Taylor in 1964, leading to their being frequently called 'Taylor cones'. This theory yields an expression for the charge density σ (C m^{-2}) at the interface, which is compatible with the observed onset voltages for cone formation. But Taylor's cone must necessarily have an angle $\alpha_T = 49.29°$, in contradiction to experiments, where other values are observed (Hayati, Bailey & Tadros 1987*a*, *b*). An extension of Taylor's analysis with a simple model incorporating the space charge field due to the spray (Fernández de la Mora 1992) has recently relaxed the paradoxical impossibility of cone angles $\alpha < \alpha_T$. The model assumes that the droplets are small enough for their inertia to be negligible, and that the spray is a cone of angle β whose apex coincides with that of the meniscus. It predicts a relation $\alpha(\beta)$, which is in acceptable agreement with measurements for the case of sprays of submicron droplets. In less conductive liquids,

where jets as long as the cone basis d_n separate the meniscus from the spray, the existence of sharply conical menisci with $\alpha \neq \alpha_T$ (see figure 1, and the photograph in Fernández de la Mora & Gomez 1993) remains unexplained.

The present investigation is on the basic mechanisms and scaling laws controlling the current emitted by Taylor cones, which bears directly on the amount of charge carried by the spray droplets. Its organization is the following. Section 2 describes a preliminary experimental exploration showing that the current transmitted by relatively conducting electrified liquid cones is nearly independent of electrostatic boundary conditions (voltages and electrode shapes). This study reveals also what appears to be a square-root dependence $I \sim Q^{\frac{1}{2}}$ between the spray current I and the liquid flow rate Q. A few measurements of jet diameters d_j show that they scale with a certain characteristic length $r^* \sim Q^{\frac{1}{2}}$. Section 3 offers a preliminary explanation for this behaviour, indicating further that the characteristic quantity $I^* \sim (\gamma KQ/\epsilon)^{\frac{1}{2}}$ is an appropriate measure for the current carried by the jet (ϵ and γ are, respectively, the dielectric constant of the liquid and the coefficient of interfacial tension). Section 4 describes a detailed experimental study of the dependence of the emitted current on the quantities K, Q and ϵ, where all the data are found to be represented approximately by $I = f(\epsilon)(\gamma KQ/\epsilon)^{\frac{1}{2}}$. Section 5 takes further the analysis of section 3 to yield the internal electric field and surface shear stresses in the conical region far from the apex. It also studies the asymptotic limit $\epsilon \gg 1$, in which an upper bound is found for the current I_s carried by convection of surface charge near the apex. This bound accounts only for one-quarter of the measured current, implying that much of the jet current is still transported by conduction in the apex region. The validity of some of the hypotheses made is assessed in §6, while §7 collects the main conclusions.

2. Preliminary experimental observations

Let us define the 'electrospray current' I as the charge streaming from the cone tip per unit time. Let us also, for definiteness, choose a configuration in which the charged liquid is held at the exit of a metal capillary needle (figure 1*c*) facing perpendicularly a flat grounded electrode. The volumetric flow rate Q of liquid ejected through the jet can accordingly be controlled by supplying it through the needle. The quantity I we wish to characterize could depend on, among other variables,

(i) liquid flow rate Q;

(ii) liquid properties such as viscosity coefficient μ, electrical conductivity K, density ρ, dielectric constant ϵ, mobilities f^+ and f^- of the dissolved ions, etc., interfacial tension coefficient γ;

(iii) distance between the electrodes and diameter of the high-voltage needle holding the liquid;

(iv) voltage difference V between the capillary needle and the ground electrode;

(v) properties of the gas: the density and viscosity affect negligibly the motion of the meniscus and the jet, though they may affect the drift of the spray droplets towards the ground plate. The dielectric constant is taken to be unity. The resistance to electrical breakdown is ignored since a cone jet forms only in the absence of gas discharges. The electrical conductivity of the gas is thus negligible.

2.1. *Irrelevance of the spray and the electrostatic variables at high conductivities*

Remarkably enough, for all the liquids tested with conductivities K roughly in the range of 10^{-4} S m^{-1} and above, we find that, as long as a stable cone can be formed and Q is held constant, I is practically independent of the needle voltage V, or the geometry

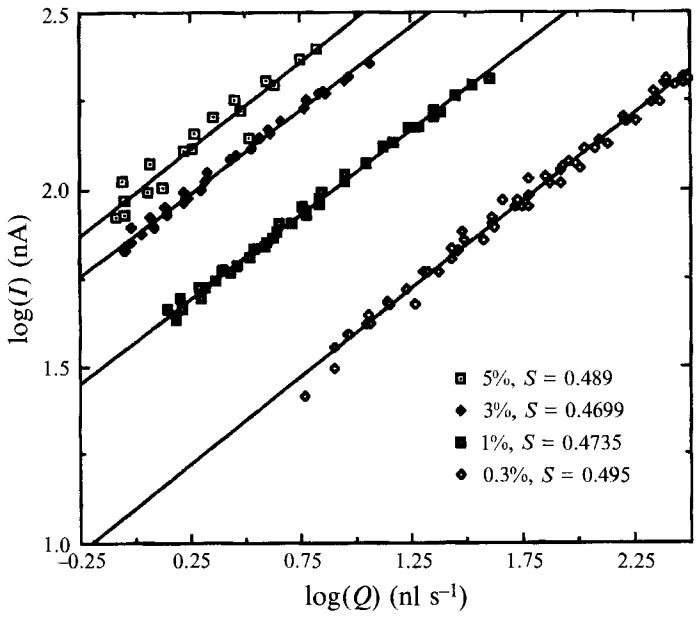

FIGURE 2. Log–log plot of the spray current I *vs.* flow rate Q for 1-octanol seed with various volume fractions of sulphuric acid, as indicated by the symbols. The data for 0.3% acid contain three $I(Q)$ curves at $V = 4$, 4.5 and 5 kV, which are practically indistinguishable from each other. S is the regression slope $\mathrm{d}\ln I/\mathrm{d}\ln Q$ (solid lines).

of the electrodes. For the case of dioxane seeded with formamide, Cloupeau & Prunet-Foch (1989) have reported curves $I(Q)$ for which I becomes decreasingly dependent on needle voltage at increasing conductivities. Such behaviour is illustrated in figure 1 (*a*, *b*) for the case of ethylene glycol seeded with LiCl (10^{-4} molar; $K = 5 \times 10^{-5}$ S m^{-1}). The liquid is held on a stainless steel needle with an outer diameter of 1.07 mm and a roughly conically tapered tip ending sharply at a diameter of 0.81 mm. The currents nearly coincide in figures 1 (*a*) and 1 (*b*) with identical flow rates and electrode geometries ($I_a = 41.0$ nA; $I_b = 41.6$ nA), but rather different capillary voltages ($V_a = 5$ kV; $V_b = 3$ kV), which lead to drastically different meniscus shapes. Figure 1 (*c*) illustrates an extreme configuration where the meniscus is rather close to the ground electrode, so that the jet reaches it while still intact (or if already broken into droplets, before these have dispersed into a spray). Yet, at a fixed flow rate, the current takes nearly the same value as in the case of a more distant ground electrode reached by the liquid in the form of a spray. Figure 2 is a log–log plot of the spray current I *vs.* flow rate Q for 1-octanol seeded with various volume fractions of sulphuric acid, as indicated by the symbols. The data for 0.3% H_2SO_4 contain three $I(Q)$ curves at $V = 4$, 4.5 and 5 kV, which are practically indistinguishable from each other. Similarly, figure 3 shows the spray current versus pressure drop across the feeding line (proportional to flow rate) for two different solutions of formamide. Although each was taken with two different needles having inner/outer diameters of 0.24 mm/0.41 mm; and 0.81 mm/1.07 mm, respectively, the corresponding curves are nearly identical. The needle diameter is therefore also an irrelevant parameter.

Accordingly, for a given liquid, the $I(Q)$ curves resulting at different values of either the needle voltage V or diameter d_n, the distance between its tip and the ground plate, the meniscus shape and the spray structure, are nearly coincident. It thus appears as

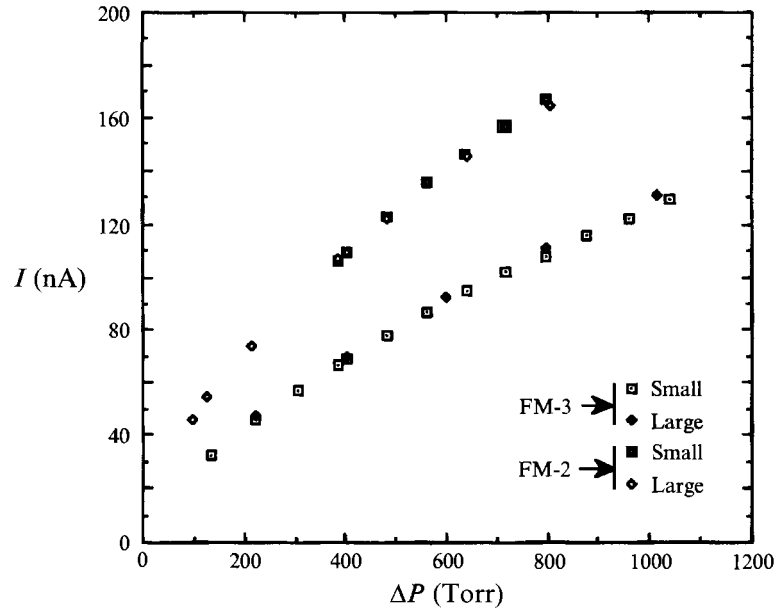

FIGURE 3. Spray current versus pressure drop across the feeding line (proportional to flow rate) for two different solutions of formamide. There are two sets of data for each solution, taken with two different needles (denoted small and large) having inner and outer diameters of 0.24 and 0.41 mm; and 0.81 and 1.07 mm, respectively. I is also independent of needle diameter.

if the cone jet were a constant-current generator, insensitive to the surrounding electrostatic environment. However, this simple behaviour does not hold in general for liquids with small electrical conductivities. Also, the domain in Q–V space in which the conical meniscus is stable does depend on electrode geometry.

2.2. *The $I \sim Q^{\frac{1}{2}}$ law for the spray current*

Equally noteworthy from figure 2 is the fact that the $I(Q)$ curves appear to be straight lines in logarithmic coordinates, with slopes enticingly close to $\frac{1}{2}$.† Such remarkable simplicity suggests an elementary current-carrying mechanism, and should greatly simplify the task of understanding charge transport in Taylor cones.

2.3. *Jet diameter*

The main thrust of the present study is on the current carried by the jet. However, it is important for the interpretation of the experiments to have some knowledge of the geometry of the jet. We have accordingly taken a series of photographs of cone jets from a solution of LiCl in ethylene glycol ($K = 5 \times 10^{-5}$ S m^{-1}) at higher magnification than in figure 1. The flow rates were in the range $0.51 \leqslant \eta \leqslant 2.01$, in terms of the dimensionless parameter η

$$\eta = [\rho K Q/(\gamma \epsilon \epsilon_0)]^{\frac{1}{2}}, \tag{1}$$

where ϵ_0 is the electrical permittivity of vacuum (taken to be identical to that of the gas). Figure 4 is a photo of the jet corresponding to the largest of these flow rates,

† This $\frac{1}{2}$ power is clearly larger than the one we infer from figure 8 of Cloupeau & Prunet-Foch (1989), whose liquid (dioxane) is considerably less conducting and polar than ours.

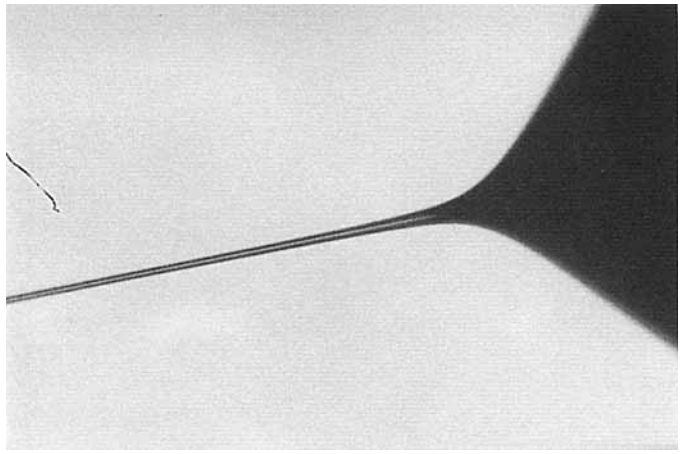

FIGURE 4. Structure of the cone jet for the same solution as figure 1 at higher magnification. The dimensionless flow rate variable (1) is $\eta = 2$ ($Re = 10.2$).

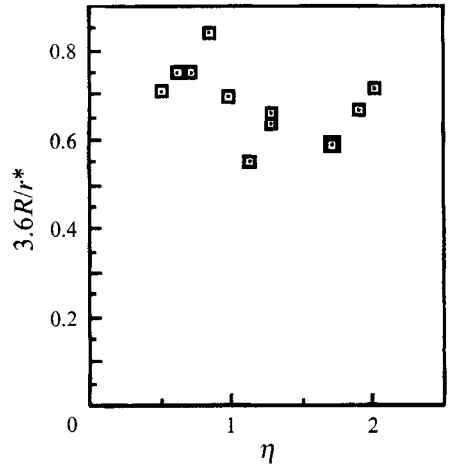

FIGURE 5. Dimensionless terminal radius $R_j = \frac{1}{2}d_j$ from photographs of ethylene glycol jets ($K = 5 \times 10^{-5}$ S m^{-1}; $1.64 < Re < 10.2$), showing that d_j scales with r^*.

which may be seen to be rather long, with a width decreasing very slowly though monotonically in the downstream direction. Although it is difficult to characterize its shrinking diameter through a single number d_j, we have done so approximately by measuring its smallest value in each photograph, with errors which may be as high as 30%. The resulting values are plotted in figure 5 as the ratio $1.8d_j/r^*$, where

$$r^* = (Q\epsilon\epsilon_0/K)^{\frac{1}{3}}. \tag{2a}$$

It is noteworthy that d_j/r^* is practically independent of η, with a value scattered around 0.4 for all cases, which justifies the scaling law

$$d_j \sim r^*. \tag{2b}$$

This finding is in marked contrast to the alternative scaling (Fernández de la Mora *et al.* 1990)

$$d_j \sim R^* = (\rho Q^2/\gamma)^{\frac{1}{3}}, \tag{2c}$$

found to fit approximately the data published by Jones & Thong (1971), Cloupeau &

Prunet-Foch (1989) and Gomez & Tang (1991*a*, *b*, 1993). These data, however, correspond to substantially smaller liquid conductivities and much larger jet Reynolds numbers than those of figure 5. The possible ranges of validity of (2*b*) and (2*c*) will be discussed in §§3.2.3 and 3.3.

3. Preliminary theoretical notions

3.1. *High-conductivity asymptote and irrelevance of electrostatic variables*

The observed limiting behaviour where I becomes independent of electrostatic parameters can be seen experimentally to arise only at relatively large electrical conductivities K (Cloupeau & Prunet-Foch 1989, figure 8). But an increasing K is known to give rise to a decreasing jet diameter d_j, as shown among others by Smith (1986), and as implied also by (2*a*, *b*). The limiting behaviour under discussion must therefore be associated with the asymptote $d_j/d_n \to 0$, where the jet diameter is exceedingly small at the scale of the diameter of the capillary tube. If the disparity between these two dimensions is sufficiently large, an intermediate region $d_n \ll r \ll d_j$ for the polar distance r from the cone apex must exist. In this domain, $r/d_n \to 0$ and $r/d_j \to \infty$ simultaneously, so that d_n and d_j both become irrelevant quantities. By realizing that this intermediate region is actually describable by Taylor's theory, V may also be shown to be an irrelevant variable. This identification could be established from pure theoretical arguments, but shall be based here mostly on observations.

When looking at the meniscus of figure 1(*b*) at the scale d_n of the capillary, one sees first a surface with a curvature of the order of d_n^{-1} which heads towards the axis, and nearly crosses it with a finite angle α. But the crossing does not take place, because, at a distance from the axis very small compared to d_n, a highly curved region appears where the jet begins to form. The intermediate region $d_n \ll r \ll d_j$ near the virtual tip where the meniscus nearly intersects the axis is therefore nothing but a Taylor cone of semi-angle α. Conversely, an electrified meniscus may have a well-defined conical shape only in the limit when $d_j/d_n \ll 1$. This is all too evident from a number of published photographs (including some of Zeleny, Taylor, Hayati *et al.*, Gomez & Tang, etc.) for moderately conducting liquids, where, rather than a cone, one sees a concave–convex surface with an inflexion point in its generatrix. Even in figure 1, with $d_n/d_j \sim 100$, the length disparity is not quite large enough for a conical region to be sharply and indubitably recognizable. However, the photographs of Fernández de la Mora (1992) for substantially more-conducting liquids (with invisible submicron jets) show liquid tips which look precisely conical to the eye.

Let us now consider a situation with $d_j/d_n \ll 1$, with a wide and sharply conical intermediate region. This region is electrohydrostatic because the electric and velocity fields associated with the finite charge and mass flow through the jet both decay as $(d_j/r)^2$ and are therefore negligible. The corresponding electric field is therefore as given by Taylor (1964) from the condition that the normal capillary and electrostatic tensions balance each other exactly at the interface. For a cone of semi-angle α (figure 6), the former is given by $\gamma/(r\tan\alpha)$. Because the electrostatic tension is $\frac{1}{2}\epsilon_0 E_\theta^2$, the equilibrating electric field normal to the cone must then be

$$E_\theta = (2\gamma/\epsilon_0 \tan\alpha)^{\frac{1}{2}} r^{-\frac{1}{2}}. \tag{3}$$

E_θ in (3) depends neither on V nor on d_n, so that the field near the apex is insensitive to the circumstances of the electrodes creating it. The jet structure would be determined by solving a certain electrohydrodynamic problem which matches upstream with (3),

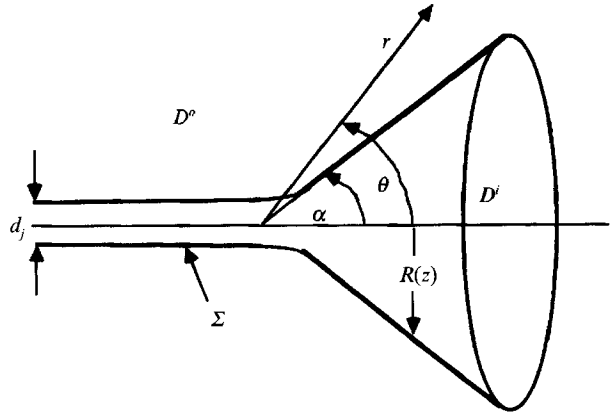

FIGURE 6. Sketch of the meniscus and the variables used for its description. D^o = outer domain (gas); D^i = inner domain (liquid); Σ = interface.

and does not, therefore, receive independent information about V or d_n. Neither the jet structure nor the current it carries may then depend directly on the external electrostatic parameters, as observed.

In conclusion, the high-conductivity limit in which the jet is extremely thin at the scale of d_n leads to a considerable simplification of the description of an electrified liquid cone. Then (and only then) the meniscus develops a clearly defined intermediate conical region between the needle and the jet. As a result, the jet structure and current become independent of electrostatic parameters. When $d_n \sim 1$ mm, this high-conductivity asymptote corresponds roughly to jet diameters below 10 μm. This range is the one where understanding electrified cone jets would be of greatest practical value, since no known alternative atomizer can produce monodisperse droplets smaller than a few microns.

3.2. *Dynamical perturbations to Taylor's theory*

The following theoretical considerations are intended to provide a preliminary explanation of the observed $I \sim Q^{\frac{1}{2}}$ law on the basis of Taylor's theory. Some of the available evidence pointing to the consistency of his explanation of the cone has been discussed by Fernándes de la Mora (1992) at the purely hydrostatic level. Our plan here is to introduce dynamical effects as small changes in Taylor's structure, and to identify the conditions under which these perturbations cease to be negligible. The exercise introduces a characteristic distance λ from the cone apex and a characteristic current I^*, which are, respectively, closely related to the observed jet radius and the current. The fact that the breakdown condition for Taylor's theory captures the two most fundamental features of the dynamical problem associated to the jet structure suggests strongly that his picture is fundamentally sound.

3.2.1. *The effect of fluid motion on the distribution of charge at the interface*

The charge density σ (C m^{-2}) at the surface of a conductor in equilibrium is such that the external electric field is normal to the interface and the internal field is null. Let us denote by σ_e the value of σ in this electrostatic limit. If the conductor is a fluid and its surface is set into motion, the flow transports the surface charge, shifting its value from σ_e. As a result, the electric field inside the liquid ceases to be zero, and electrical currents set up through it, in an attempt to restore electrostatic equilibrium. In the case of a conical meniscus carrying a net mass flow, the fluid speed is small and the conducting section large far upstream from the apex, where the perturbation on σ_e is

slight, and the small resulting currents lead to negligible potential drops. However, the situation becomes far less favourable in the vicinity of the apex, where liquid speeds are rather large and the section available for conduction small. As a result, one may expect that the fluid motion will not perturb appreciably Taylor's equilibrium except in a relatively small region near the apex. Our objective here is to determine the dimensions of this region.

Let us for the moment assume that Taylor's model for the conical meniscus is an appropriate approximation to the real problem, so that $\sigma_e = \epsilon_0 E_\theta$ is given from (3) by

$$\sigma_e = \beta r^{-\frac{1}{2}}; \quad \beta^2 = 2\gamma\epsilon_0/\tan\alpha, \tag{4}$$

where α is the cone semi-angle. In order to describe the shift of σ away from σ_e resulting from convection of the interface, one must first characterize the transport of charge down the meniscus, which proceeds by convection and conduction at the charged interface Σ, and only by conduction through the bulk. The surface current density $\boldsymbol{j}_s$ is modelled here as

$$\boldsymbol{j}_s = (\boldsymbol{u}_s + f_i \boldsymbol{E}_t^i)\sigma \quad \text{at} \quad \Sigma, \tag{5}$$

where $\boldsymbol{u}$ is the fluid velocity and $\boldsymbol{u}_s$ its value at the interface; f_i is the electrical mobility of the surface ions, and $\boldsymbol{E}_t^i$ the tangential component of the electric field $\boldsymbol{E}^i$ inside the liquid. Similarly, the bulk current density $\boldsymbol{j}_b$ is taken for a fluid with electrical conductivity K to be given by

$$\boldsymbol{j}_b = K\boldsymbol{E}^i. \tag{6}$$

The electric fields in the domains D^i and D^o inside and outside the liquid, respectively, satisfy

$$\boldsymbol{E}^k = -\nabla\phi^k; \quad \nabla^2\phi^k = 0 \quad \text{in} \quad D^k \quad (k = i \text{ or } o). \tag{7}$$

The boundary conditions at the interface Σ require that the potential be continuous, and also yield the surface charge density σ. Thus

$$\phi^i = \phi^o; \quad \sigma = \epsilon_0[\boldsymbol{E}^o - \epsilon\boldsymbol{E}^i]\cdot\boldsymbol{n} \quad \text{at} \quad \Sigma, \tag{8a, b}$$

where $\boldsymbol{n}$ is the unit vector normal to the interface directed away from the liquid.

The condition of charge conservation at Σ requires that the conduction current density striking the interface from inside be incorporated into the surface current:

$$\nabla_s\cdot\boldsymbol{j}_s = \boldsymbol{j}_b\cdot\boldsymbol{n} \quad \text{at} \quad \Sigma. \tag{9a}$$

For the case of an axisymmetric geometry characterized by a distance $R(z)$ to the axis, where z is the axial variable, defining the path length along the surface $\mathrm{d}s = \mathrm{d}z\{1+(\mathrm{d}R/\mathrm{d}z)^2\}^{\frac{1}{2}}$, (9$a$) turns into the following conservation equation for the surface current I_s:

$$I_s = 2\pi R u_s \sigma, \quad \frac{\mathrm{d}I_s}{\mathrm{d}s} = 2\pi RKE_n^i, \tag{9b, c}$$

where $u_s = \mathrm{d}s/\mathrm{d}t$ is the fluid speed at Σ along the generatrix, and the term $f_i E_r$ from (5) has been provisionally neglected in comparison to u_s (see §6.2). Equation (9c) expresses how the surface or convection current increases at the expense of the conduction current density. A useful alternative form for (9c) may be obtained by writing E_n^i in terms of E_n^o and I_s by means of (8b) and (9b). Introducing further the equilibrium current I_e, defined as the convection current I_s corresponding to the equilibrium charge density $\sigma_e = \epsilon_0 E_n^o$, (9$c$) becomes

$$t_e\frac{\mathrm{d}I_s}{\mathrm{d}t} = -(I_s - I_e), \quad \text{with} \quad \mathrm{d}t = \frac{\mathrm{d}s}{u_s}; \quad \epsilon\epsilon_0/K = t_e; \quad I_e = 2\pi R u_s \epsilon_0 E_n^o, \tag{9d–g}$$

where t_e is the electrical relaxation time, and t is the convective time. Equation (9d) is a prototypical linear relaxation equation with two limiting behaviours. In the equilibrium limit when $t_e \, \mathrm{d} \ln I_e/\mathrm{d}t \ll 1$, the solution $I_s = I_e$ is governed entirely by local properties at the interface. In the opposite limit, $t_e \, \mathrm{d} \ln I_e/\mathrm{d}t \gg 1$, I_s is incapable of tracking the changes of I_e, so that its value depends on the full past history of I_e. In what follows, we shall call 'charge relaxation phenomena' those arising when $t_e \, \mathrm{d} \ln I_e/\mathrm{d}t$ is not small. A measure of their importance is given by the ratio between t_e and the characteristic flow time.

Let us now consider the implications of (9) in the near-equilibrium region where the surface is a cone of angle α and E_n^o is given to a first approximation by (3). In order to make further progress, some knowledge of the velocity field is required. As a first and very tentative approach, we take it to be the spherically symmetric 'sink':

$$\boldsymbol{u} = U\boldsymbol{e}_r; \quad U = -a/r^2; \quad a = \frac{Q}{2\pi(1-\cos\alpha)}; \quad r \to \infty. \tag{10}$$

This velocity field is in fact the average convective disturbance of the interface for a given flow rate Q. In reality, the presence of electrical shear stresses may produce surface flows larger than a/r^2, so that (10) represents the minimal possible convective disturbance. The description (10) will be shown in §6.3 to hold at small jet Reynolds numbers, though it evidently fails in the apex region where the cone turns into a jet.

Accepting (10) provisionally, the flow time t in (9e) is immediately found as $r^3/3a$. The condition for the onset of charge relaxation phenomena is therefore that $3at_e/r^3 \sim 1$, which introduces the characteristic electrical relaxation length $\lambda = (3at_e)^{\frac{1}{3}}$:

$$\lambda^3 = \frac{3Qt_e}{2\pi(1-\cos\alpha)}; \quad \{\lambda = 1.187\,(Qt_e)^{\frac{1}{3}} \quad \text{for} \quad \alpha = \alpha_T = 49.29°\}. \tag{11a, b}$$

Except for its dependence on α through a factor close to unity, λ coincides with the length r^* introduced in (2a) as the characteristic measure of the jet diameter observed experimentally.

In conclusion, when Taylor's model is complemented with a sink flow, as the fluid approaches the cone apex and r becomes small, the velocity increases according to (10) and relaxation phenomena set in at a distance λ from the apex. The coincidence between the jet scaling length r^* and the electrical relaxation length λ also strongly suggests that the formation mechanism for the jet is associated with charge relaxation phenomena.

3.2.2. *The characteristic convection current*

When $r \gg r^*$ and $\sigma \to \sigma_e$, the surface current I_s associated to the convection of surface charge tends to $I_e = 2\pi r \sin\alpha \, u_s \sigma_e$, given asymptotically by

$$I_s \to I^* x^{-\frac{3}{2}}; \quad (x = r/\lambda \gg 1), \tag{12a}$$

$$I^{*2} = \frac{2\pi \sin 2\alpha}{3(1-\cos\alpha)} \frac{\gamma Q K}{\epsilon}; \quad [I^* = 2.44\,(\gamma K Q/\epsilon)^{\frac{1}{2}} \quad \text{for} \quad \alpha = \alpha_T], \tag{12b, c}$$

indicating that, at the point where charge relaxation becomes non-negligible, the convected current I_s is a quantity of the order of $(\gamma KQ/\epsilon)^{\frac{1}{2}}$. It is noteworthy that I^* scales with $Q^{\frac{1}{2}}$, as found experimentally for the spray current in §2. The more detailed measurements of §4 will show further that the spray current scales approximately as $(\gamma KQ/\epsilon)^{\frac{1}{2}}$, with a proportionality factor which depends on ϵ. The fact that the

breakdown conditions for Taylor's static theory capture the essential features of the two fundamental dynamic quantities of this problem strongly suggests that his model contains the essence of the statics of the problem, and remains valid nearly down to the jet development region.

3.2.3. *Jet diameter and fluid inertia*

The experiments discussed in §2.3 showed that the jet diameter d_j may scale either with the electrical relaxation length r^* or alternatively with the length R^* of (2*c*), depending on the circumstances. The characteristic quantity R^* is actually of the order of the value of r at which Taylor's theory breaks down as a result of fluid inertia. Indeed, the balance between the capillary and the electrostatic tensions fails as soon as the dynamic pressure $\frac{1}{2}\rho u^2$ becomes comparable with γ/r. For a given liquid flow rate Q, this happens when r is a few times smaller than R^*, as in (2*c*). In other words, when inertia is significant, a conical meniscus cannot remain in equilibrium in the region $r < R^*$, and must accordingly adopt a different geometry, presumably a jet. It thus seems that the formation of the jet may be determined either by inertia or by charge relaxation, depending on which of these two phenomena acts first as the cone apex is approached. Interestingly enough, the key ratio R^*/r^* is simply related to the dimensionless flow rate introduced in (1):

$$R^*/r^* = \eta^{\frac{2}{3}}. \tag{13}$$

Accordingly, when η is smaller than unity inertia has no chance of becoming relevant, so that $d_j \sim r^*$. In the opposite limit $\eta \gg 1$ one could expect the alternative behaviour $d_j \sim R^*$. However, it is conceivable that for flows dominated by viscosity inertia might still remain irrelevant at relatively large values of η. In any case, if the flow in the cone were spherically symmetric as in (10), it would be irrotational, and viscous effects would drop entirely out of the picture. As a result, even for a relatively small jet Reynolds number Re (defined here based on its final diameter d_j near the break-up region, and on the fluid density ρ and coefficient of viscosity μ)

$$Re = 4\rho Q/(\pi d_j \mu), \tag{14}$$

it is unlikely that inertia will remain irrelevant at large enough η. In conclusion, it seems reasonable to adopt (2*b*) in the limit of either sufficiently small Reynolds numbers or small enough η, while (2*c*) would probably hold at large Re and large η. With our present limited knowledge of this problem it is not possible to establish how large η must be for a given Re for the transition between (2*b*) and (2*c*) to occur. Nonetheless, the present work is concerned mostly with the high-conductivity limit in which the jet diameter is very small, which tends to coincide with the $Re \ll 1$ limit. Furthermore, values of η will always be smaller than 10, so that (2*b*) is most likely to apply, as shown in figure 5 for $\eta \leqslant 2$. Work in progress by Rosell-Llompart & Fernández de la Mora (1994) shows for $Re < 1$ that (2*b*) is a fair approximation for $\eta < 8$, though not as good for $\eta > 2$ as for $\eta < 2$. Because in the high-conductivity limit d_j is only a few times smaller than r^*, one may write an explicit expression for Re in terms of only Q and fluid properties. Alternatively, we define another Reynolds number Re^* based on r^*, which differs from Re only by a factor near three,

$$Re^* = \frac{Q^{\frac{2}{3}}}{\nu t_e^{\frac{1}{3}}}, \tag{15}$$

where $\nu = \mu/\rho$ is the kinematic viscosity of the liquid. Re^* has the advantage over Re

of involving only externally supplied parameters. Its value for the data of figure 5 is in the interval $0.506 \leqslant Re^* \leqslant 3.15$.

3.3. *Dimensionless representation*

For a problem where the relevant externally controlled physical magnitudes are Q, γ, ρ, ϵ, ϵ_0, μ and K, the current I and the jet diameter d_j must have the form

$$\frac{I}{\gamma(\epsilon_0/\rho)^{\frac{1}{2}}} = \xi(\epsilon, \eta, Re^*); \quad \frac{d_j}{R^*} = \Omega(\epsilon, \eta, Re^*), \tag{16a, b}$$

where ξ is I made dimensionless with the characteristic current $\gamma(\epsilon_0/\rho)^{\frac{1}{2}}$, while η and Re^* have been defined in (1) and (15). The variable η can also be interpreted as the characteristic current $(\gamma QK/\epsilon)^{\frac{1}{2}}$ made dimensionless with $\gamma(\epsilon_0/\rho)^{\frac{1}{2}}$. η^2 is also the ratio of the flow time formed by the volume $\rho Q^2/\gamma$ divided by Q (a sort of transient time over a characteristic inertial length R^*) and the electrical relaxation time.

In the limit of sufficiently small Re^* and of moderate values of η, where inertia becomes irrelevant, ρ would drop out of the picture and one could write

$$\frac{I}{(\gamma KQ/\epsilon)^{\frac{1}{2}}} \to f(\epsilon, Z); \quad \frac{d_j}{r^*} \to \Gamma(\epsilon, Z) \quad \text{as} \quad Re^* \ll 1. \tag{17a, b}$$

In the Appendix it is shown that the quantity

$$Z = \frac{\gamma t_e^{\frac{2}{3}}}{\mu Q^{\frac{1}{3}}} \tag{17c}$$

measures the radial variations in the axial velocity profile of the jet. These are due to electrical shear stresses which tend to make the liquid velocity larger at the surface than at the core, while viscosity has the opposite tendency, towards making the axial velocity radially uniform.

In conclusion, (16*a*) shows that the ratio between I and the current I^* of (12) is in principle a function of the parameters ϵ, η and Re^*, which degenerates into a function, (17*a*), of only Z and ϵ in the low-Reynolds-number limit (provided η is not too large). A similar statement may be made with respect to d_j/r^*. It is not obvious *a priori* why the viscous parameter Z would be irrelevant.

4. Experimental

Section 3.2 has identified K and Q as probably the most important parameters entering in this problem. We therefore proceed to study experimentally their effect on I for several liquids.

4.1. *System and measurement routine*

The experimental set-up is fairly standard, as sketched in figure 7. The meniscus is held at the end of a stainless steel capillary needle connected to a high-voltage power supply at a positive potential V. Facing the needle perpendicularly is a flat ground electrode, kept in most experiments at 9 mm from the end of the needle. Two needles were used, with outer and inner diameters of 1.07 mm and 0.81 mm, and 0.41 mm and 0.24 mm, respectively. Both have an approximately conically tapered end, finishing relatively sharply at the inner diameter. The smallest one was used for all experiments, except for those with 1-octanol and those reported in relation to figures 1 and 2. The capillary tube is enclosed in a sealed cylindrical metallic chamber in order to be able to control

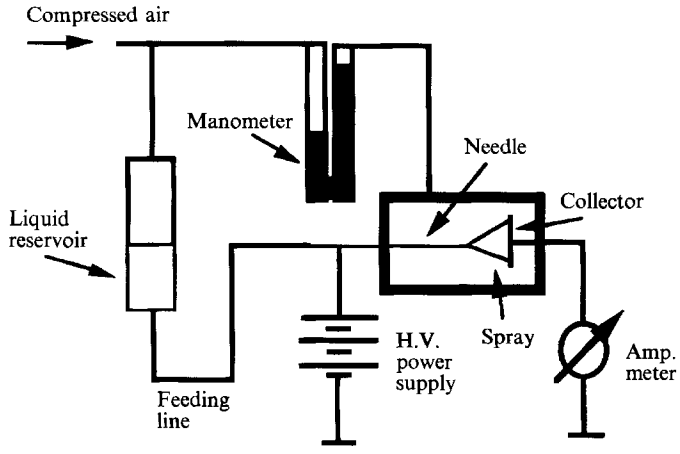

FIGURE 7. Sketch of the experimental setup.

the surrounding atmosphere, always kept near laboratory conditions of temperature and pressure. This feature was essential for the experiments with water, whose large surface tension requires relatively large electric fields for a cone to form. As a result, discharges in air tend to appear at voltages smaller than those necessary for the meniscus to become conical, though this problem may be avoided in gases with a higher breakdown potential such as CO_2 (Zeleny 1915), SF_6 (Smith 1986), etc. All tests with water were accordingly carried out in CO_2. Water is also by far the most volatile of all the solvents used. Accordingly, had the amount of material evaporating from the meniscus not been negligible in relation to the total flow rate Q, the measured volume of liquid fed to the needle would have differed from that ejected through the jet. In order to reduce this potential problem, evaporation was minimized by using the smallest needle diameter. Its negligible importance was verified by observing that the reduction of the evaporation rate brought about by saturating the chamber with water vapour did not change the $I(Q)$ curves. The current was measured by placing an electrometer between the electrode collecting the spray and ground.

The liquid was fed into the metal capillary by a narrow insulating tube connected to a reservoir (typically a 5 cm^3 disposable syringe). Its flow rate Q was controlled by imposing a pressure difference ΔP across the feeding line. In order to keep Q strictly linear in ΔP, ΔP was substantially larger than the pressure jump between the atmosphere in the chamber and the liquid inside the meniscus (of the order of $4\gamma/d_n$, where d_n is the inner diameter of the needle). Also, the meniscus was kept at the same height as the free surface of the sample liquid. ΔP was measured with a mercury or an oil manometer as the difference in pressures between the gas pushing the liquid and that in the spray chamber. The actual flow rate was inferred in some of the experiments from the linear relation between Q and ΔP, after determining the ratio $Q/\Delta P$ at a relatively large flow rate. Q was found by introducing a bubble into the liquid line and measuring its velocity at a given ΔP. The line consisted most often of a Teflon tube with an inner diameter of 0.3 mm and lengths ranging from several metres down to some 10 cm. For the smaller flow rates, fused silica tubes typically shorter than 10 cm and with inner diameters between 50 μm and 75 μm were used instead. In some cases, the full relation Q *vs.* ΔP was measured and confirmed to be linear. This method of flow measurement was required because of the very small values of Q characteristic of such conductive liquid cones, typically in the range of 10^{-6} cm^3 s^{-1}, and smaller than 10^{-7} cm^3 s^{-1} in one case. The approach leads to extremely stable cones, but is not free

	1-Octanol	Water	BA	EG	TEG	Formamide
γ (dyn cm^{-1})	26.06	72.58	39.96	48.4	45.2	58.35
ϵ	10.34	80.1	13.1	38.66	23.69	111.0
μ (cP)	10.64*	1.0019	7.76*	21.0	49.0	3.764
ρ (g cm^{-3})	0.8255	0.9982	1.04927*	1.11	1.123	1.13

TABLE 1. Macroscopic properties of the pure solvents used in this work at 20 °C (* at 15 °C) (Riddick *et al.* 1986). γ = surface tension coefficient, ϵ = dielectric constant, μ = viscosity coefficient and ρ = density. BA = benzyl alcohol; EG = ethylene glycol; TEG = triethylene glycol.

from problems, as the silica line is not completely inert with all solutions, particularly with saline water. As a result, partial clogging, or variations of flow resistance with time were not uncommon, and might have resulted in experimental errors. The Teflon tube generated highly reproducible results, but the smallest diameter of 0.3 mm found commercially was too wide to be suitable at the smallest flow rates or with the least-viscous substances. Extending this work to conductivities in the range of 10 or 100 S m^{-1} (and flow rates as small as 10^{-9} cm^3 s^{-1}) promises to be rewarding, but will surely present some serious experimental challenges.

The spray chamber was provided with two glass windows for monitoring visually the meniscus and associated spray, to ensure that a stable cone-jet regime (Cloupeau & Prunet-Foch 1989) was present. This verification was carried out occasionally under continuous light through an optical microscope, generally just before and after measuring each $I(Q)$ curve.† Any change of operating conditions was easily detected through jumps or instabilities in the measured current. It is also important to be sure that the current is transmitted mostly by the jet and not by a corona discharge. This is easily confirmed within our regime of operation by the independence of the spray current of voltage, as corona discharges exhibit a marked dependence between these two variables. Such symptoms arose occasionally for the liquids with the highest surface tensions, and appeared even with 1-octanol at the largest conductivities tried (10% H_2SO_4). In such cases, any observable effect of a gaseous discharge on total current was eliminated by running the spray in CO_2 rather than in air.

In order to achieve the highest reproducibility and stability it is essential to eliminate gas bubbles from the liquid samples (in our case by prior immersion in an ultrasonic bath), and also to keep the needle connecting the disposable syringe reservoir with the liquid line free from bubbles. Because the liquid viscosities and electrical conductivities depend substantially on temperature, high-precision results are only attainable by carrying out the measurements in a thermal bath. This study, however, was done at room temperature, monitored with a thermometer. The calibration $Q(\Delta P)$ and the measurement of the conductivity were done immediately after the end of each experiment. The temperature never varied by more than 0.5 °C through the data collection period, so that no corrections were introduced to account for this effect.

Liquids. Equation (16*a*) suggests that the fundamental physical variables governing the spray current are ϵ, ρ, μ, γ, Q and K. The role of γ is relatively well known (Smith 1986), so that this parameter was ignored in the selection of fluids. In order to operate in the high-conductivity regime where electrostatic parameters are irrelevant, it is important that K be relatively large. This is most readily (though not exclusively) achieved with relatively polar solvents, which in this study cover the range $10 < \epsilon < 110$.

† In order to avoid increasing the liquid temperature above ambient conditions, the illumination lamp was on only as briefly as possible.

Solution	Concentration (mol l^{-1})	K (S m^{-1})	Π_μ
EG-1	0.96	0.24	0.0737
EG-2	0.23	6.26×10^{-2}	0.115
EG-3	4.2×10^{-2}	1.69×10^{-2}	0.178
EG-4	1.0×10^{-3}	5.0×10^{-4}	0.577
EG-5	1.0×10^{-4}	5.4×10^{-5}	1.21
FM-1	0.147	0.27	0.64
FM-2	1.47×10^{-2}	5.49×10^{-2}	1.088
FM-3	1.47×10^{-3}	3.16×10^{-2}	1.309
FM-4	—*	2.84×10^{-2}	1.35
W-1	9.98×10^{-2}	0.83	1.646
W-2	9.98×10^{-3}	9.26×10^{-2}	3.42
W-3	9.98×10^{-4}	2.13×10^{-2}	5.58
W-4	9.98×10^{-5}	2.15×10^{-3}	11.98
TEG-1	1.0	4.5×10^{-2}	0.45
TEG-2	3.87×10^{-2}	4.38×10^{-3}	0.0977
1-8ol-1	0.047	1.16×10^{-3}	0.122
1-8ol-2	0.13	5.67×10^{-3}	0.196
1-8ol-3	0.38	2.3×10^{-2}	0.332

TABLE 2. Conductivity K and molar concentration (mol of solute per l of solvent) for the various solutions for which $I(Q)$ curves have been measured: EG = ethylene glycol; TEG = triethylene glycol; FM = formamide; W = water; 1-8ol = 1-octanol. Also one solution of benzyl alcohol 0.17N having an electrical conductivity K of 0.0079 S m^{-1} was studied. All solutions used LiCl as the salt, except those with 1-octanol, which were seeded with H_2SO_4. (*) as purchased.

(*a*) N (LiCl–EG)	0.966	0.23	8.9×10^{-2}	4.2×10^{-2}
$100^*\Delta\gamma/\gamma$	2.3	1.16	0.58	0.58
(*b*) N (LiCl–Water)	1.36	1.87	2.67	3.82
$100^*\Delta\gamma/\gamma$	2.26	3.46	5.121	7.6

TABLE 3. Effect of solute concentration N (mol l^{-1} of solvent) on γ: (*a*) measured data for LiCl in ethylene glycol; (*b*) LiCl in water, Weast (1980).

Except for water, an important selection criterion was that the liquid vapour pressure be relatively small. The solutions used involved H_2SO_4 in 1-octanol and LiCl in benzyl alcohol, ethylene glycol, triethylene glycol, formamide and water. Except for water, all the solvents were used as purchased (HPLC grade when available). Formamide had a substantial electrical conductivity (0.028 S m^{-1} as purchased), and was not purified further. As a result, the nature and concentration of the ions is unknown for the least-conducting sample of this solvent (FM-4). Water was distilled and de-ionized. The literature values of the fundamental properties (γ, ϵ, μ, ρ) of these pure solvents are shown in table 1 (Riddick & Bunger & Sakano 1986).

The solutions for which data are reported, are characterized in table 2 with respect to solute concentrations and conductivities. Given the relatively high polarity of most of these liquids, their conductivities could be varied over a considerable range. Absolute values of the surface tension coefficients were not measured for the pure substances. In the case of ethylene glycol, the value of γ relative to that of the pure solvent was measured for the solutions, with results shown in table 3 (γ increases with salt concentration). γ was found to change by at most 2.3% at the highest concentration of 0.966 moles of LiCl per litre of solvent. The effect is even smaller for

N	Water + LiCl ϵ (18 °C)	Water + LiCl ϵ (25 °C)	Formamide + $LiNO_3$ ϵ (25 °C)
0.0	81	—	110
0.05	79	—	—
0.2	76.5	—	—
0.31	—	73.2	—
0.5	71.5	71.2	97
0.62	—	68.4	—
0.93	—	64	—
1.00	66.5	64.2	88
1.50	—	57	—
2.00	56.8	51	73
3.00	49.3	—	—
4.00	—	50	—
5.00	39.1	—	—
8.00	—	39	—
12.00	—	35	—

TABLE 4. Dielectric constant ϵ versus solute concentration, from Akhadov (1981). N = moles of solute per litre of solvent.

water solutions, where the published relative change in γ is 2.26% for a 1.36 molar solution of LiCl (Weast 1980). Accordingly, literature values for the pure substances were used for γ in the data reduction, and an identical practice was followed regarding ρ. The same simplification would lead to larger errors if practised for the dielectric constant ϵ, as shown in table 4 for water and formamide, where 1 molar solutions of LiCl are seen to produce changes in ϵ larger than 10%. Unfortunately we are not equipped to measure ϵ in conducting liquids, so that the data reduction has also been based on the pure fluid value of ϵ, which leads to unknown and perhaps non-negligible errors for the most conductive solutions in all the solvents used. In the case of water (also for formamide to a lesser degree), the variation of ϵ in the range of conductivities covered was only a few percent. This favourable circumstance follows from the small viscosity and high dielectric constant of these solvents, for which rather high conductivities result even from the relatively dilute solutions for which ϵ is close to the value at infinite dilution.

4.2. *Experimental results*

To give an idea of the range of variation of the physical magnitudes involved in this study, figure 8 shows raw data of measured currents *vs.* flow rates for many of the substances and conductivities studied. Notice, however, that the data shown in each curve do not necessarily cover the full range of flow rates at which the cone jet is stable. Finding the minimum flow rate and current is exceedingly time consuming for highly conducting solutions. The highest flow rate is more readily determined. But it depends on the electrode configuration, and has therefore no universal significance. All data collected are shown in figure 8 except for three of the curves for 1-octanol shown in figure 2, where the characterization of conductivities and temperatures was not as careful as with the other substances. All of these data may be accurately described by power laws $I \sim Q^n$ with an exponent n which departs slightly from $\frac{1}{2}$, more in some cases than in others. The points corresponding to water deserve special attention, because their data reduction is not clouded by indeterminacies in the value of ϵ. The corresponding I *vs.* $(\gamma QK/\epsilon)^{\frac{1}{2}}$ curves are shown in figure 9, where all the data points for

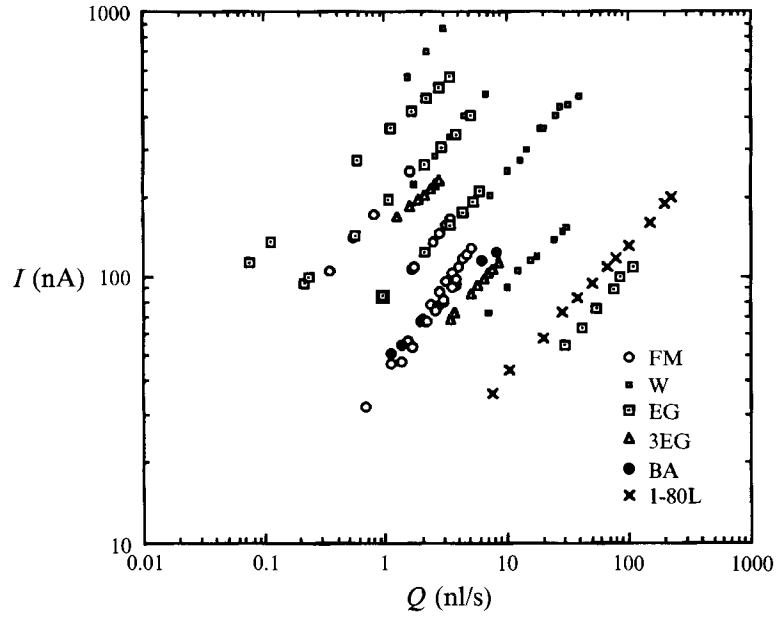

FIGURE 8. Raw data on spray current I *vs.* liquid flow rate Q for various solutions. For symbols see table 2.

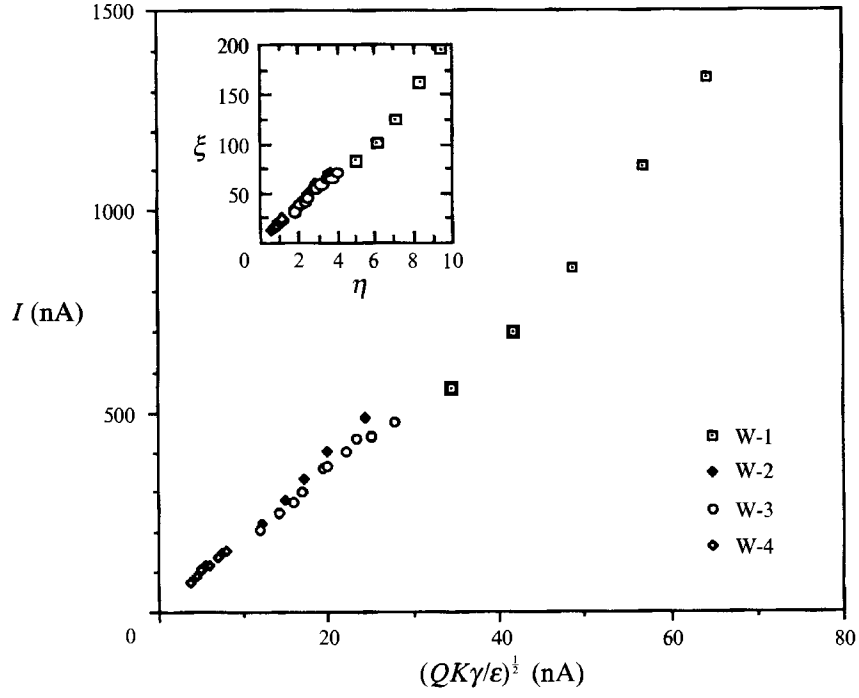

FIGURE 9. Spray current I versus $(QK\gamma/\epsilon)^{\frac{1}{2}}$ for water solutions. The same data are shown in the inset in dimensionless coordinates ξ, η (equations (16*a*) and (1)).

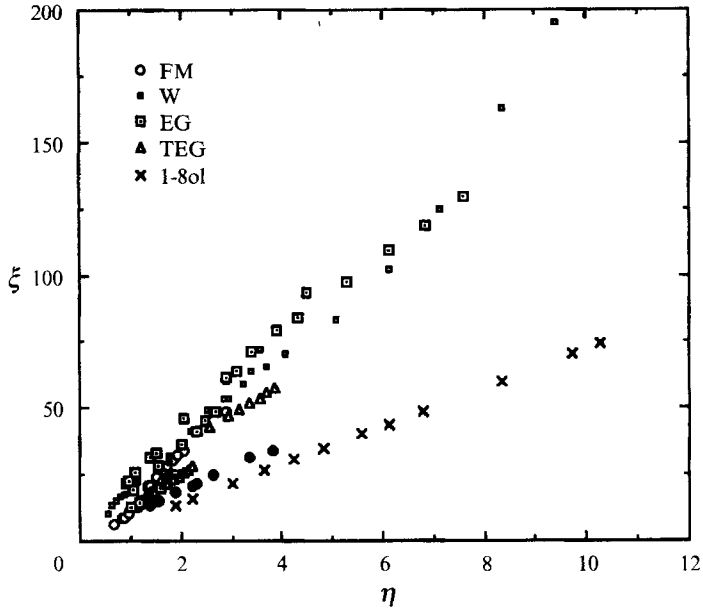

FIGURE 10. Dimensionless spray current ξ versus η (equations (16a) and (1)) for a variety of solutions.

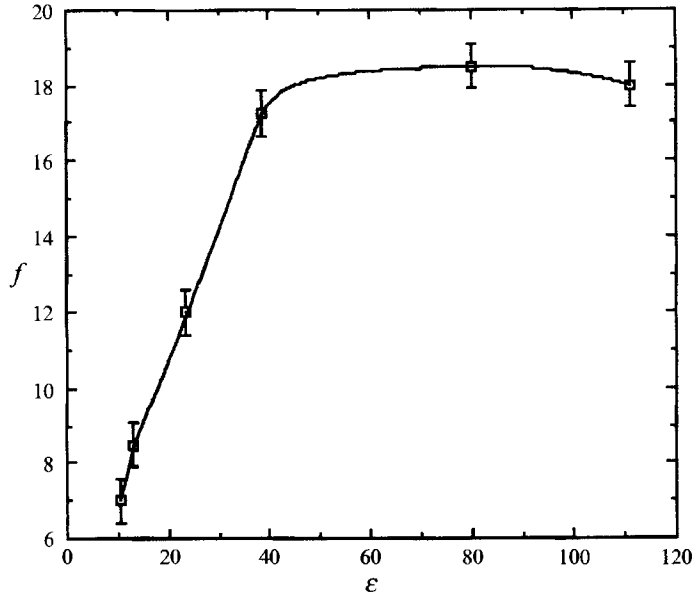

FIGURE 11. Slope $f = \mathrm{d}\xi/\mathrm{d}\eta$ of the lines of figure 10 *vs.* dielectric constant ϵ for the pure solvents.

conductivities that vary 400-fold collapse into a single and approximately linear curve. The inset shows the same data in the dimensionless form $\xi(\eta)$ suggested by (16a). Interestingly enough, Re^* appears to be an irrelevant variable.

All the points from figure 8 are re-plotted in figure 10, also in the form $\xi(\eta)$, though the value of ϵ used for the reduction is that corresponding to the pure solvent. The data

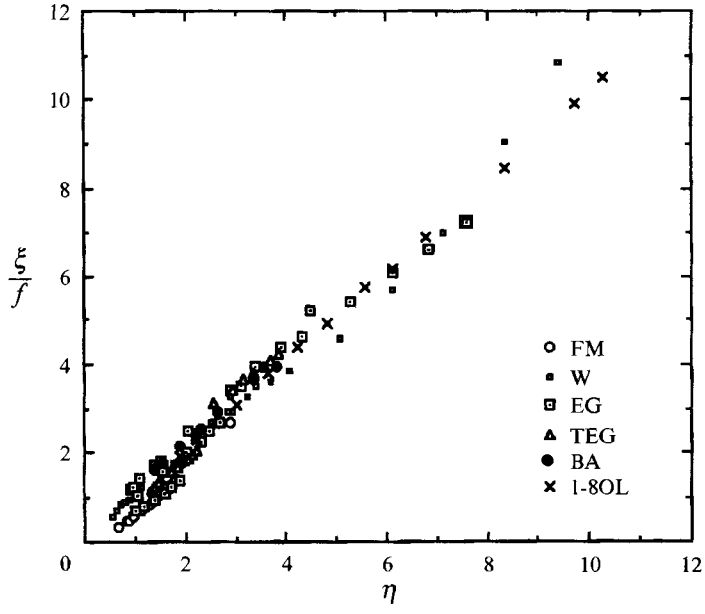

FIGURE 12. Dimensionless spray current ξ divided by f *vs.* η (equations (16*a*) and (1)).

for each substance collapse approximately onto a single straight line going through the origin, though with a scatter which, for some species, becomes relatively important at the smallest currents. The curves associated with the different substances spread into a fan of distinct lines, with slopes $\mathrm{d}\xi/\mathrm{d}\eta$ increasing from 1-octanol to water and formamide, in order of increasing values of the dielectric constant. The slope $f(\epsilon) = \mathrm{d}\xi/\mathrm{d}\eta$ obtained from linear regression of the data for each solvent is plotted in figure 11 as a function of ϵ (pure solvent value). The points may be joined through a relatively continuous curve characterized by a plateau value near 18 for $\epsilon > 40$, and a rapid decrease in $f(\epsilon)$ for smaller dielectric constants. Figure 12 plots ξ normalized with $f(\epsilon)$ as a function of η, with most of the points now falling reasonably close to the diagonal line $\xi/f = \eta$. One is therefore led to the approximate experimental result

$$\xi = f(\epsilon)\,\eta \quad \text{or} \quad I = f(\epsilon)\,(\gamma K Q/\epsilon)^{\frac{1}{2}}. \tag{18a, b}$$

4.3. *Discussion*

A first remarkable feature of (18) is the conspicuous absence of the viscosity coefficient. The current simply scales with the quantity I^* of (12) through an ϵ-dependent factor.

In addition, the data of figures 10 to 12 contain the independent and rather interesting result that η_{min} is of order unity for all the substances studied. A detailed experimental investigation of the scaling laws for the minimum flow rate Q_{min} at which Taylor cones are stable is still pending, as is a theory accounting for the existence of this lower stability boundary.† Nonetheless, it seems reasonable at this stage to accept provisionally the limited available empirical evidence that $\eta_{min} \sim 1$, in order to simplify further the interpretation of (18).

† For the least-conducting solutions of water and formamide studied, we find that this lower boundary corresponds quite closely to the maximum possible ratio of I/Q when the emitted jet contains only ions of one polarity, the counter-ions having precipitated entirely in the metal capillary.

Notice that the variables Re^* and Z may be rewritten in terms of η and the quantity Π_μ as

$$\Pi_\mu = (\gamma^2 \rho t_e)^{\frac{1}{3}}/\mu; \quad Re^* = \eta^{\frac{4}{3}} \Pi_\mu; \quad Z = \eta^{-\frac{2}{3}} \Pi_\mu, \tag{19a–c}$$

where Π_μ depends only on the liquid properties and not on the flow rate. Accordingly, if η is typically larger than one, Z will be typically smaller than Π_μ and Re^* at any flow rate. Therefore, Re^* and also Z become irrelevant quantities in the low-Reynolds-number limit. Values of Π_μ are shown in table 2 for all the solutions used in this work. They are at most near unity except for the case of aqueous solutions. The result (18) could accordingly be understood as a small-Π_μ limit where both Re^* and Z become irrelevant and (17) degenerates to

$$\frac{I}{(\gamma K Q/\epsilon)^{\frac{1}{2}}} \to f(\epsilon); \quad \frac{d_j}{r^*} \to \Gamma(\epsilon) \quad \text{as} \quad \Pi_\mu \ll 1, \tag{20a, b}$$

approximately as observed. The puzzling thing is that (20a) also holds for the water solutions, which are definitively not in the low-Reynolds-number range.

The noticeable departure of some of the data in figure 12 from the diagonal (particularly at smaller values of η) may be due in part to errors in the measurement of the very small flow rates involved (as discussed earlier), and also to possible variations of ϵ away from the pure fluid value. However, much of this spread is not due to noise in the data, but to systematic departures from the scaling law $I = f(\epsilon)(\gamma Q K/\epsilon)^{\frac{1}{2}}$. This can be seen in figure 8 from the raw data, some of whose logarithmic slopes $\mathrm{d}\ln I/\mathrm{d}\ln Q$ differ from $\frac{1}{2}$. In spite of these inaccuracies, the predictive power of (18b) is undeniable for all the substances tried and for a range of conductivities and flow rates spanning some four orders of magnitude. Of course, much remains to be done before (18) might be considered solidly verified. Wide as it is, the range $0.83 > K > 5 \times 10^{-5}$ S m^{-1} of conductivities explored is still a narrow fraction of the interval bound between liquid-metal conductivities and those of semiconducting liquids, for which these results presumably hold. Also, only six substances have been studied, and none with a dielectric constant smaller than 10. The characterization of $f(\epsilon)$ is therefore incomplete. Figure 11 should also be taken as provisional until the values for many more solvents are added to it.

5. Further theoretical considerations

5.1. *Far field $r \gg r^*$*

By incorporating into Taylor's theory the perturbations brought about by fluid motion, we have found in §§3.2.1 and 3.2.2 the magnitude of the characteristic length λ at which relaxation effects set in, as well as the characteristic value of the current associated with surface convection. The same formulation can be used in the equilibrium region $r \gg r^*$ to infer the asymptotic form of the electric field and the electrical shear stresses. Knowledge of these quantities will make it possible to judge the self-consistency of the various hypotheses made (the sink-flow assumption, in particular).

Let us consider again the near-equilibrium portion of the meniscus, shaped as a cone of angle α, with E_n^o given to a first approximation by (3). Equation (9a) may be written for this case in spherical polar coordinates r, θ as

$$\frac{\partial}{\partial r}(r\sigma u_s) = rKE_\theta^i \quad \text{at} \quad \theta = \alpha, \tag{21}$$

where we maintain the sink-flow description (10) for the fluid velocity $\boldsymbol{u}$. We introduce the following dimensionless form of E_θ^o at $\theta = \alpha$, which tends to unity at large r (β was defined in (4)):

$$F = \epsilon_0 E_\theta^o r^{\frac{1}{2}}/\beta \quad \text{at} \quad \theta = \alpha, \tag{22}$$

and also the dimensionless internal field and polar radius, Ψ and x, respectively:

$$\Psi = \epsilon\epsilon_0 E_\theta^i \lambda^{\frac{1}{2}}/\beta \quad \text{at} \quad \theta = a; \tag{23}$$

$$x = r/\lambda. \tag{24}$$

After making use of (8*b*), (10) and (22)–(24), (21) takes the simple form

$$\frac{1}{3x}\frac{\mathrm{d}}{\mathrm{d}x}\left[\frac{1}{x}(\Psi - Fx^{-\frac{1}{2}})\right] = \Psi, \tag{25}$$

while the surface charge is given by

$$\sigma = \sigma_e(F - \Psi x^{\frac{1}{2}}). \tag{26}$$

Accordingly, the perturbation on σ due to the motion is negligible provided that F remains close to 1 and Ψ much smaller than $x^{-\frac{1}{2}}$. This is what happens in the far field $x \gg 1$, where Ψ may be obtained from (25) under the assumption that $F = 1$ and that $\Psi = 0$ on its left-hand side. This leads to

$$2\Psi \to x^{-\frac{7}{2}} \quad (x \gg 1). \tag{27}$$

Equation (27) is consistent with the assumptions made (slight departures from Taylor's results) provided that x^3 is a large quantity. This is assured when r is a few times larger than λ, which confirms our more qualitative result (11). In physical variables, (27) reads

$$E_\theta^i \to \frac{3Q(2\gamma\epsilon_0/\tan\alpha)^{\frac{1}{2}}}{4\pi K(1-\cos\alpha)} r^{-\frac{7}{2}} \quad \text{at} \quad \theta = \alpha \quad (r \gg \lambda). \tag{28}$$

The corresponding electrical potential within the liquid is accordingly given by the Legendre function P of order $-\frac{5}{2}$ (or, equivalently, $\frac{3}{2}$) which is regular at the axis of symmetry inside the cone. But because its associated field decays too fast to be able to carry a current, ϕ^i must be complemented by a radial conductive contribution proportional to I/r, which dominates the field for $r \gg \lambda$:

$$\phi^i \to \frac{-1}{4\pi K(1-\cos\alpha)\, r}\left\{2I + 3Q\frac{(2\gamma\epsilon_0)^{\frac{1}{2}}}{(r^3\tan\alpha)^{\frac{1}{2}}}\frac{P_{\frac{3}{2}}(\theta)}{P'_{\frac{3}{2}}(\alpha)}\right\} \quad (r \gg \lambda). \tag{29}$$

It is therefore clear that the current is carried entirely by conduction in the hydrostatic region $x \gg 1$, even though the potential variations driving it are produced by convection in the apex region. Further downstream, relaxation phenomena arising in the region $x \sim 1$ drive a fraction of this flow of charge (of the order of $(\gamma QK/\epsilon)^{\frac{1}{2}}$) towards the surface, converting it into the convection current.

5.2. *A model for the convection current in the limit* $\epsilon \gg 1$

The case of liquids with a high dielectric constant produces considerable simplifications in the analysis because ϕ^0 and the shape of the meniscus differ then by quantities of the order of $1/\epsilon$ from those when no currents flow through the cone. As a result, the meniscus remains conical and F, defined in (22), stays near unity through much of the relaxation region $x \sim 1$.

The limit $\epsilon \gg 1$ is often encountered in practice, being inescapable for the high-conductivity conditions considered in the present paper. Indeed, making highly conductive electrolytes requires that dissolved species be dissociated into small ions, but because dissociation energies are typically much higher than thermal energies, this process is impossible at room temperature unless the solvent is sufficiently polar to provide the needed electrical screening. The associated problem is simplified considerably for the following reasons:

(i) According to (8*b*), changes of order $1/\epsilon$ in E_n^i lead to changes of order unity in the surface charge σ, and thus in the surface current I_s. Consequently, ϕ^i may be at most of order $1/\epsilon$, in which case equation (8*a*) implies that, to lowest order in $1/\epsilon$, $\phi^o = 0$ at Σ. The meniscus surface is therefore nearly equipotential, even in the presence of substantial internal currents.

(ii) If E^i is of order $1/\epsilon$, then the normal electrical stress $\boldsymbol{T}\cdot\boldsymbol{n}$ on the interface, given by

$$\boldsymbol{T}\cdot\boldsymbol{n} = \tfrac{1}{2}\epsilon_0 [E_n^{o2} - \epsilon E_n^{i2} - (1-\epsilon) E_t^2] \quad \text{at} \quad \Sigma, \tag{30a}$$

remains unmodified to lowest order from the equipotential value, even when currents flow inside the cone:

$$\boldsymbol{T}\cdot\boldsymbol{n} = \tfrac{1}{2}\epsilon_0 E_n^{o2} [1 + O(1/\epsilon)]. \tag{30b}$$

This holds true even if the charge density σ undergoes a substantial relative shift with respect to its electrostatic value σ_e.

(iii) Accordingly, to lowest order in $1/\epsilon$, the external problem is uncoupled from the internal field E^i and from the surface or bulk currents. Taylor's description for the meniscus (a cone) and the external field (3) thus remains valid through much of the relaxation region $x \sim 1$. In term of the variable F defined in (22), this implies that F is close to unity not only in the far field $x \gg 1$, but also at values of x comparable to 1 or even smaller.

5.2.1. *Model of an infinitely thin jet*

Let us make the arbitrary (though instructive) assumption that the jet radius is much smaller than r^*, so that the meniscus is conical down to its apex. As a result, when $\epsilon \gg 1$, Ψ may be obtained by solving (25) with $F = 1$, yielding

$$\Psi = -xi(x) + x^{-\frac{1}{2}}; \tag{31}$$

$$i(x) = -\exp(x^3) \int_{\infty}^{x^3} e^{-y} y^{-\frac{1}{2}} dy. \tag{32}$$

The convection current $I_s(x) = -2\pi r \sin\alpha \sigma U$ may then be written as

$$I_s(x) = I^* i(x), \tag{33}$$

where I^* was defined in (12). Because $i(x)$ in (32) asymptotes towards $\pi^{\frac{1}{2}}$ as $x \to 0$, I_s converges to a constant as the apex is approached:

$$I_s(0) = I^* \pi^{\frac{1}{2}}. \tag{34a}$$

In the case when $\alpha = \alpha_T = 49.29°$, (34*a*) yields

$$I_s = 4.331 (\gamma Q K/\epsilon)^{\frac{1}{2}} \quad (\alpha = \alpha_T = 49.29°). \tag{34b}$$

The picture is therefore the following. As shown in (29), conduction is the main carrier of charge in the far field $x \gg 1$. Eventually, electrical relaxation phenomena arising in the region $x \sim 1$ convert a fraction of this flow of charge (of the order of $(\gamma Q K/\epsilon)^{\frac{1}{2}}$) into

convection current. So far these results are not restricted by the requirements that $\epsilon \gg 1$ or that the jet be infinitely thin. When these two hypotheses are added, one reaches the additional conclusion that I_s is frozen at a value given by (34) as the cone tip is approached. Notice, however, that this prediction for I_s is some four times smaller than the spray current found experimentally in the limit $\epsilon \gg 1$ ($f(\epsilon) = 18$ according to figure 11, *vs.* 4.33 in (34*b*)).

5.2.2. *An upper limit for the convective current at the cone apex*

The discrepancy found between the measured spray current and I_s as given by (34*b*) could in principle be attributable to the following deficiencies of the model. First, the jet radius is not negligible at the scale of r^*. It is some 0.2 times r^* for the case of ethylene glycol, and it is unlikely that it will be much smaller for more polar liquids. Secondly, although the region of validity of Taylor's field extends below $x = 1$, it does not quite reach $x = 0$ because, among other reasons, the meniscus eventually ceases to be equipotential (§6.5).

However, one can argue heuristically that (34*b*) actually yields an upper limit for the convective current near the apex. Indeed, I_e and I_s (defined in (9)) increase monotonically as the apex is approached, and because I_e is the driving force for I_s in (9*d*), a reduction in I_e will lead to a reduction in I_s. However, in the presence of charge relaxation I_e is most probably smaller than otherwise, because relaxation tends to decrease E_n^0 with respect to the purely electrostatic value. This is evident from figure 4, where the curvature at the head of the jet is smaller than the corresponding value for a cone. But because $\boldsymbol{T}\cdot\boldsymbol{n}$, is proportional to this curvature, (30b) shows that the prevailing values of E_n^0 and I_e are necessarily smaller than in Taylor's theory. The actual value of I_s at the virtual apex would therefore be smaller than predicted by (34*b*). The consequence is that more than three-quarters of the current at the head of the jet is still carried by conduction. Because the jet is long and slender (some 100 final diameters typically), it is very likely that this conduction current will eventually reach the surface, to become convection current. But this must happen in the jet and not in the cone.

6. Limits of validity of the analysis

The following basic hypotheses have been used through this study without rigorous justification (other more restrictive assumptions, $\epsilon \gg 1$ for instance, brought for special cases have already been discussed):

(i) Taylor's description applies in the region far from the apex;
(ii) charge transport is modelled by (5) and (6);
(iii) the ion mobility term in (5) is small compared to the convective term;
(iv) the flow is described by a sink at the cone apex.

Our objective here is to assess when these assumptions are justified.

6.1. *Taylor's theory*

As pointed out in the introduction, the paradoxical formation of liquid cones with angles smaller than Taylor's may be rationalized for highly conducting liquids, and thus the use of (3) is in principle consistent with the limit $d_j/d_n \ll 1$ considered in this work. But, in practice, the hypothesis is questionable in a substantial fraction of our experimental conditions for moderately conducting liquids whose jet is as long as the cone. There is accordingly no rigorous justification of (3) for many of the experiments in which the $I \sim Q^{\frac{1}{2}}$ law appears nonetheless to hold. On the other hand, the results

Ion	H^+	K^+	Na^+	Li^+	OH^-	Cl^-
$f_i(f/\epsilon)\,(\rho/\epsilon_0)^{\frac{1}{2}}$	0.864	0.182	0.124	0.095	0.486	0.189
$10^8 f_i$	36.3	7.62	5.19	4.01	20.52	7.91

TABLE 5

Liquid	1-octanol	water	benzyl-OH	ethylene glycol	3ethylene glycol	formamide
ϵ	10.34	80.1	13.1	38.66	23.69	111
$f(\epsilon)$	7	18	8.4	17.3	12.1	18
$\dfrac{K f(\epsilon)\rho^{\frac{1}{2}}}{n_0 e\ 3\epsilon\epsilon_0^{\frac{1}{2}}}$	0.0011	0.177	0.0015	0.009	0.0020	0.137

TABLE 6

found experimentally for I and d_j agree with the scaling parameters I^* and r^* suggested in §3.2 on the basis of (3), lending therefore further support to Taylor's description.

6.2. *Ion mobility parameters*

The term $f_i E_r^i$ has been ignored in relation to u_s in the surface current density (5) entering into the charge balance equations (9) and (21). It is therefore necessary that the characteristic value of the ratio $f_i E_r^i/U$ be small. Using the far-field expression for $E_r^i \sim I/r^2$, and (18) for I, one finds

$$f_i E_r^i/U = f_i I/(KQ) = f_i(f/\epsilon)(\rho/\epsilon_0)^{\frac{1}{2}}\eta^{-1}. \tag{35}$$

But, because η takes values typically larger than unity,

$$(f_i E_r^i/U)_{max} \sim f(\epsilon)(f_i/\epsilon)(\rho/\epsilon_0)^{\frac{1}{2}}. \tag{36}$$

Typical values of $f(\epsilon)(f_i/\epsilon)(\rho/\epsilon_0)^{\frac{1}{2}}$ and f_i (in $m^2 V^{-1} s^{-1}$ from Moore 1972) for various ions in water at 298.15 K are shown in table 5. The effect is accordingly quite important for H^+ and OH^- in water, but represents at most a 20% correction ($\eta_{min} = 0.5$) for the Li salts used in this work, and substantially less at flow rates well above the minimum. The magnitude of this effect for the other solvents (for which we do not know f^+) may be estimated by using $f^+ + f^-$ instead and estimating roughly the value of $(f^+ + f^-)/f^+$ as $\frac{1}{3}$ as in the case of LiCl in water. $f^+ + f^-$ may be inferred from the measured conductivity and the known salt concentration n_0 on the assumption that the salt is fully ionized ($f^+ + f^- = K/en_0$; e = elementary charge). The values shown in the last row of table 6 are all for the solvent–salt combinations of table 2 at the smallest concentration of salt shown for each. The electrical drift velocity of the surface ions thus represents at most a 20% correction in the worst of the cases, and is negligible for most of our experiments.

6.3. *Limits of validity of the sink-flow hypothesis*

Following (11) r^* has been interpreted as the lengthscale at which charge relaxation phenomena set in only under the assumption that the fluid moves as in a spherical sink, which is not always true. Indeed, numerous observations are available of fluid circulation inside Taylor cones, where the liquid descends towards the apex along the cone surface, and returns towards the capillary tube along its axis (Hayati *et al.* 1986).

Liquid	1-octanol	water	benzyl-OH	ethylene glycol	3ethylene glycol	formamide
K^*_{1mm} (S m^{-1})	2.1×10^{-6}	3.11×10^{-3}	9.87×10^{-6}	4×10^{-6}	4.5×10^{-7}	1.68×10^{-4}

TABLE 7

It is evident in such cases that most of the fluid motion is not associated with the sink flow (10) (which cannot lead to a retrograde motion along the axis). Instead, the circulation is generally attributed to electrical shear stresses arising at the cone surface. Let us now find a criterion for such a shear-induced motion to become insignificant.

Assuming that the liquid velocity in the meniscus is given by a sink flow, the corresponding complete description of the radial electric field and the surface charge at $r \gg r^*$ make it straightforward to evaluate the far field of the shear stress $\tau_{\theta r} = \tau = E_r \sigma$, and check under what circumstances it leads to negligible effects on the sink flow (10). For $r \gg r^*$, E_r^i is dominated by the I/r^2 conductive contribution, while the surface charge σ is given by Taylor's result (4). Therefore,

$$\tau = \frac{(\gamma\epsilon_0)^{\frac{1}{2}} I}{K r^{\frac{5}{2}}} \frac{1}{\pi(1-\cos\alpha)(2\tan\alpha)^{\frac{1}{2}}}; \quad r \gg r^*. \tag{37}$$

In the limit when viscous forces dominate over inertia, this shear leads to a velocity $U_\tau \sim \tau r/\mu$, whose relative importance with respect to the basic sink flow $U = -a/r^2$ may be written as

$$\frac{U_\tau}{U} \sim \frac{f(2\gamma\rho r/\tan\alpha)^{\frac{1}{2}}}{\mu\epsilon\eta}, \tag{38}$$

where we have put $I = f(\rho K Q/\epsilon)^{\frac{1}{2}}$. Alternatively, if inertia were to dominate over viscous forces, the shear-driven surface velocity would be given instead by $U'_\tau \sim \tau\delta/\mu$, δ being the thickness of the thin boundary layer through which the surface shear would be transmitted to the bulk fluid. But, because in this case $\delta \ll r$, it follows that $U'_\tau \ll U_\tau$, so that the ratio U_τ/U in (38) represents an upper bound for the relative importance of the shear-induced flow. This group (38) is by no means negligible when r is of the order of the needle diameter and $\eta \sim 1$. Using $r = 1$ mm, and $\tan\alpha = 1$, (38) takes values ranging from 85.7 in water down to 3.28 in triethylene glycol, for the fluids used in this work. Still, the corresponding Reynolds number $Re_\tau = \tau r^2\rho/\mu^2$ may be written (except for an α-dependent factor close to 1) as

$$Re_\tau = \eta K^*/K, \text{ with } K^* = f\epsilon_0\mu^{-2}(\gamma^3\rho/r)^{\frac{1}{2}}.$$

K^* is tabulated in table 7 for the solutions used in this work, taking $r = 0.1$ cm. K^*_{1mm} is smaller or, occasionally, comparable with the actual experimental conductivities. As a result, Re_τ is typically of order one or smaller in our experimental runs, so that it would be straightforward to calculate the correction U_τ to the flow. It is also clear that the high-Reynolds-number regime leading to vigorous circulation may also be easily attained, for instance, with water at conductivities of some 10^{-6} S m^{-1}. In any case, in the region of interest, where $r = r^*$ we find that

$$\{U_\tau/U\}_{r^*} \sim Zf/\epsilon, \tag{39}$$

where the viscous parameter Z was defined in (31c). The criterion for the shear effects to be negligible, and for U to be given by the sink flow (9) is that

$$Zf/\epsilon \ll 1. \tag{40}$$

Otherwise, the analysis must be modified to incorporate shear-induced motion. Because $f/\epsilon < 1$ and η is of order one or larger for all the experiments in this study, (40) is automatically verified when Re^* is of order unity or less, as required for the jet inertia to be negligible in the region $r \sim r^*$. Accordingly, if Re^* is small, Z is also small, and shear-induced motion is negligible in the relaxation region $x \sim 1$.

6.4. *Limits on the validity of the model used for conduction*

The conduction model (6) implicitly takes K to be uniform throughout the liquid, a hypothesis that becomes questionable near the surface. Indeed, the interface provides a reservoir of charge of one polarity only (say positive, for a positively charged meniscus). Accordingly, it may absorb the incoming positive charge brought in by conduction from the bulk, but it cannot inject back into the bulk the negative charge needed to maintain neutrality. As a result, a 'sheath' region virtually devoid of ions is created on the liquid in the neighbourhood of the interface. In order to compute the thickness of this layer, we assume first that its thickness δ is small: $\delta \ll r$, so that the far-field description of ϕ^i given in (29) holds everywhere except in that sheath. For $r(\theta-\alpha) \gg \delta$, the field E_{θ^i} is unperturbed by the sheath, so there is a net flow of negative charge $E^i_\theta n_0 f^-$ away from the sheath into the liquid. In order to maintain neutrality, an identical flow of positive charge must be expelled from the sheath into the interface. Similarly, the flow of positive charge from the bulk into the sheath is $n_0 f^+ E^i_\theta$, which, by continuity also reaches the boundary. The flow of charge to the wall is thus $n_0(f^+ + f^-) E^i_\theta$, exactly as in the absence of the sheath. This growing layer acts therefore merely as the reservoir of negative charge drawn by the field into the interior, and (6) remains effectively valid except within the narrow de-ionized region. In this case, ignoring Brownian diffusion, the shear boundary is given by the trajectory of a negative ion originating at $\theta = \alpha$ and $r \to \infty$ in the combination of electric and fluid flows (29) and (10) for $x \gg 1$. One finds

$$\theta(x) - \alpha = \frac{[4\pi(1-\cos\alpha)]^{\frac{1}{2}}}{(3\tan\alpha)^{\frac{1}{2}}} \frac{1}{\eta x^{\frac{3}{2}}} \frac{f^-(\rho/\epsilon_0)^{\frac{1}{2}}}{\epsilon}, \tag{41}$$

where the first fraction is a numerical constant of order unity (1.12 for $\alpha = \alpha_T$). The discussion from §6.2, where $f^-(\rho/\epsilon_0)^{\frac{1}{2}}/\epsilon$ was seen to be substantially smaller than $1/f(\epsilon)$ in all cases except for H^+ and OH^- ions, makes it clear that the angular width of this sheath is rather small in the cone. The analysis ignoring the presence of the sheath is therefore excellent even down to the region $r \sim r^*$ ($x \sim 1$). Further downstream, within the jet, when most of the current has incorporated itself into the surface at the expense of growth of the sheath, the cross-section of this de-ionized domain will still occupy a negligible fraction of the cross-section of the jet, except for water and formamide near the smallest achievable flow rates.

6.5. *Is the cone nearly equipotential?*

The argument used in §5.2 to show that the meniscus is equipotential with errors $O(1/\epsilon)$ was somewhat weak. It showed only that $E^i_n/E^o_n = O(1/\epsilon)$, providing no direct information on E_t to ensure that $E_t/E^o_n \ll 1$, as really required. This ratio may now be calculated in the far field using (3) for E^o_n, the I/r^2 purely conductive expression for E_r, and (18) for I. One finds

$$\frac{E_t}{E^o_n} = \frac{(\tan\alpha)^{\frac{1}{2}}}{[12\pi(1-\cos\alpha)]^{\frac{1}{2}}} \frac{f(\epsilon)}{\epsilon} x^{-\frac{3}{2}}; \quad x \gg 1, \tag{42}$$

where the leading numerical factor takes the value 0.3017 for $\alpha = \alpha_T$. We thus

encounter the surprising fact that the ratio is not just measured in units of $1/\epsilon$, owing to the relatively large factor $0.3f(\epsilon)$ in the expression. In the case of water ($\epsilon = 80$; $f = 18$), the result is $E_t/E_n^o = 0.068x^{-\frac{3}{2}}$ ($\alpha = \alpha_T$), which is acceptably small at $x = 1$, but not so small (0.76) at $x = 0.2$. Because the current is scaled up over $(\gamma KQ/\epsilon)^{\frac{1}{2}}$ by the large factor $f(\epsilon)$, the net result is that, even for some of the most polar usual solvents such as water and formamide, ϵ is not large enough for the meniscus to be equipotential well below $x = 1$. In the photograph of the ethylene glycol jet shown in figure 4, the departure from a conical shape becomes noticeable at $r = 1.8\lambda$ (λ based on $\alpha = \alpha_T$ is 20 μm; r is measured from the virtual apex, as sketched in figure 6). At $r = 1.2\lambda$, the meniscus has already departed from a straight line by some 10% of r. If the meniscus is already slightly non-equipotential at $r = \lambda$, one would expect that the electrical normal stress would have already started to be smaller than in Taylor's analysis. In this case the curvature would also have to be reduced in order to maintain mechanical equilibrium, which provides a simple inertialess mechanism for jet formation.

6.6. *Comparison with earlier observations and theories*

The important experimental results of Cloupeau & Prunet-Foch, Gomez & Tang, and Jones & Thong have already been discussed. They correspond to a regime where inertia is considerable and $\epsilon \sim 2$. But the bibliography on electrified conical menisci contains many somewhat less systematic and extensive reports on spray currents under a variety of circumstances. Many of these measurements appear to contradict each other, probably because such menisci can form under more than one regime, as discussed most lucidly by Cloupeau & Prunet-Foch (1990). For instance, Kidd (1968) describes the case of glycerol solutions ($K \sim 0.005$ S m^{-1}) electrosprayed in vacuo where the spray current is practically independent of liquid flow rate in the range $4 \times 10^{-9} < \rho Q < 10^{-7}$ kg s^{-1}. However, his mode of operation involved very high capillary voltages, at which many conical tips form around the metal rim. Pfeifer & Hendricks (1968) have published a large amount of data on charge to mass ratios q/m for droplets electrosprayed (in vacuo) from glycerine doped with NaCl. It is interesting that they find the experimental result $q/m \sim (K/Q)^{0.429}$, amounting to $I \sim K^{0.429}Q^{0.571}$, which does not differ much from our own $I \sim (KQ)^{\frac{1}{2}}$. These authors have also contributed a model incorporating ad hoc the ratio of the flow time over the electrical relaxation time, and have assumed that the emitted droplets were charge to one half of the Rayleigh limit.† The result was a prediction $I \sim K^{\frac{3}{7}}Q^{\frac{4}{7}}$, which also does not differ much from our $\frac{1}{2}$ power law. We do not know if their corresponding menisci had only one cone or many, nor was there a description of the dependence of current on voltage at fixed flow rate. More recently Tang & Kebarle (1991) have studied the effect of liquid conductivity and ion molar conductance on electrosprayed currents from water–methanol mixtures. They found that I depends on conductivity but not on ion mobility in the solvent. However, their results are only for one rather large value of $Q = 20$ μl/min, at which they find that $I \sim K^{0.22}$. The substantial discrepancy with our own observations is most likely because they operate in a rather different regime, as indicated by the value of η^2 in their work, which, for the case when $K = 0.22$ S m^{-1}, is nearly two orders of magnitude higher than the maximum at which we have been able to form a stable conical meniscus with any fluid.

† This hypothesis is based on an 'energy minimization principle', which has no rigorous basis for dissipative systems such as cone jets. We know now from the work of Jones & Thong (1971), Gomez & Tang (1991*a*, *b*, 1993), and others, that the ratio of droplet charge to the Rayleigh limit charge may be larger than $\frac{1}{2}$, as well as smaller, depending on the flow rate. Interestingly, for a problem where the droplet diameter scales with r^* and the current with I^*, the average ratio of droplet charge to Rayleigh's limiting value is a constant independent of flow rate, though perhaps varying with ϵ.

7. Conclusions

The following main conclusions can be drawn from this study on charge transfer in highly conducting electrified liquid cones.

(i) At conductivities large enough for the jet to be much thinner than the needle diameter d_n, cone jets emit currents which do not depend on the electrostatic variables. Combining the conditions $\eta \sim 1$ and $d_j \sim (Qt_e)^{\frac{1}{3}}$, the required criterion for 'high conductivity' may be written as

$$(\gamma t_e^2/\rho)^{\frac{1}{3}}/d_n \ll 1. \tag{43}$$

(ii) Ion mobilities are nearly irrelevant parameters under most conditions, with the exception of the most polar fluids at the smallest flow rates, where a 20% effect of the finite mobility of Li^+ may arise. The effect would be several times larger for more mobile ions such as H^+ and OH^-.

(iii) At sufficiently small jet Reynolds numbers the liquid flow is well approximated by a spherical sink, and charge relaxation phenomena arise at distances from the cone apex of the order of $r^* = (Qt_e)^{\frac{1}{3}}$. Then, dimensional analysis shows that the jet terminal diameter scales roughly as r^*, and the spray current as $I = f(\epsilon)\ (\gamma QK/\epsilon)^{\frac{1}{2}}$. These predictions are in agreement with observations, from which $f(\epsilon)$ is determined (figure 11).

(iv) The current I_s associated with convection of the charged interface is also of the order of $(\gamma QK/\epsilon)^{\frac{1}{2}}$ when $r \sim r^*$. An upper limit for I_s near the apex may be computed in the limit $\epsilon \gg 1$, yielding only one-quarter of the observed spray current. At least three-quarters of the flow of charge must therefore reach the head of the jet by conduction.

(v) The previous scaling law for I also holds in several instances when Re^* is not small, and this behaviour remains to be rationalized.

(vi) The three characteristic quantities R^*, r^* and I^*, with which the jet diameter and the magnitude of the emitted current scale, arise from breakdown conditions for Taylor's theory when perturbed by a sink flow. This provides further evidence on the correctness of his description of the hydrostatics of electrified liquid cones.

(vii) This work has been restricted to a particular configuration where the liquid tip is supported on a tube and the flow rate Q is controlled externally. However, because our conclusions are independent of geometrical and electrostatic details away from the cone tip, they apply far more generally, even in cases where Q is not controllable directly. There are numerous circumstances when Q is determined by relatively complex and still unresolved phenomena, such as when a liquid cone forms on a free droplet, on a droplet standing over a solid surface, or even on the free surface of a liquid pool. Even so, the relation $I(Q)$ ought to remain unchanged in many such cases, because the region near the tip which determines the jet structure can only sense global quantities such as fluid properties, Q and I. Accordingly, the flow rate associated with such situations could be inferred from (18) and a measurement of the current.

We are greatly indebted to Professor J. B. Fenn for many suggestions and ideas. Numerous discussions with Mr J. Rosell-Llompart and Professor A. Gomez of Yale, Craig Whitehouse of Analytica (Branford, Connecticut) and Professors Barrero, Fernández Feria and Gañán of the University of Seville are also gratefully acknowledged. The criticisms of Dr J. Mestel from Imperial College, London have led to considerable improvements in this text. This work has been supported by a Goodyear cooperative grant from the State of Connecticut and Analytica of Branford, and by Grants CTS-9106619 and CTS-9112601 from the US National Science Foundation.

Appendix. Lubrication-theory description of the jet

The jet emitted from the conical meniscus is rather long and slender. It may therefore be described approximately via lubrication theory, as if its velocity were mostly axial, with a parabolic radial profile. Let ξ and z be the radial and axial variables, respectively, in cylindrical coordinates, and let the radius of the jet be $R(z)$ and $u(z,\xi)$ its axial velocity. We introduce the dimensionless axial velocity v and jet width y as

$$v = \pi R^2(z)\, u(z,\xi)/Q; \quad y = \xi/R(z),$$

in terms of which the main assumption of the lubrication approximation is

$$v = a(z) + y^2 b(z).$$

The conditions that the electrical shear stress τ be given at $y = 1$ approximately by $\mu(\partial u/\partial\xi)$ and that the total flow rate be Q, yields a and b so that

$$v = 1 + C(y^2 - \tfrac{1}{2}); \quad C = \frac{\pi R^3 \tau}{2\mu Q}.$$

The axial pressure gradient is given by

$$\mathrm{d}p/\mathrm{d}z = 2\tau/R.$$

Let us now evaluate the quantity C, measuring the departure of the velocity profile from flatness. One must accordingly estimate the magnitude of the stress $\tau = \sigma E_t$, where σ is related to I_s through (9*b*). For a slender jet, E_t is given approximately by E_z, which may be treated as uniform across each section, and is thus simply related to the conduction current I_c. Accordingly

$$I_s = (1 + \tfrac{1}{2}C)\, 2Q\sigma/R, \quad I_c = \pi R^2 K E_t.$$

Introducing now the dimensionless surface and bulk currents of order one,

$$i_s = I_s/I; \quad i_c = I_c/I,$$

where I is the total spray current which we describe through (18), one obtains

$$C(1 + \tfrac{1}{2}C) = \frac{\gamma R^2}{\mu Q}\frac{i_s i_c f^2}{4\epsilon}.$$

But the group $\gamma R^2/(\mu Q)$ is equal to $Z(R/r^*)^2$, and is therefore of the order of Z. In the case of water, $f^2/(4\epsilon) = 1.01$. Finally $i_s i_c = i_s(1 - i_s)$ is at most $\frac{1}{4}$, tends probably to zero at large values of z/r^*, and would be $\frac{3}{16}$ at the head of the jet if i_s took the value $\frac{1}{4}$ there, as suggested at the end of §5.2. The conclusion is that Z provides a rough measure for C, and thus, when Z is small, the axial velocity profile will be nearly flat.

REFERENCES

AKHADOV, Y. Y. 1981 *Dielectric Properties of Binary Solutions. A Data Handbook*. Pergamon.

BAILEY, A. G. 1988 *Electrostatic Spraying of Liquids*. Wiley.

BENASAYAG, G. & SUDRAUD, P. 1985 In situ high voltage TEM observations of an EHD source. *Ultramicroscopy* **16**, 1–8.

CLOUPEAU, M. & PRUNET-FOCH, B. 1989 Electrostatic spraying of liquids in cone-jet mode. *J. Electrostat.* **22**, 135–159.

CLOUPEAU, M. & PRUNET-FOCH, B. 1990 Electrostatic spraying of liquids: main functioning mode. *J. Electrostat.* **25**, 165–184.

FENN, J. B., MANN, M., MENG, C. K., WONG, S. K. & WHITEHOUSE, C. 1989 Electrospray ionization for mass spectrometry of large biomolecules. *Science* **246**, 64–71.

FERNÁNDEZ DE LA MORA, J. 1992 The effect of charge emission from electrified liquid cones. *J. Fluid Mech.* **243**, 561–574.

FERNÁNDEZ DE LA MORA, J. & GOMEZ, A. 1993 Remarks on the article 'Generation of micron-sized droplets from the Taylor cone'. *J. Aerosol Sci.* **24**, 691–695.

FERNÁNDEZ DE LA MORA, J., NAVASCUÉS, J., FERNÁNDEZ, F. & ROSELL-LLOMPART, J. 1990 Gencration of submicron monodisperse aerosols in electrosprays. *J. Aerosol Sci.* **21**, special issue, S673–S676.

GABOVICH, M. D. 1984 Liquid-metal emitters. *Sov. Phys. Usp* **26**, 447–455.

GOMEZ, A. & TANG, K. 1991*a* Characterization of low flow rate high charge density electrosprays. In *Proc. Fifth Intl Conf. on Liquid Atomization and Spray Systems, ICLASS-91* (ed. H. Semerjian) NTIS Special Publication 813, pp. 771–778.

GOMEZ, A. & TANG, K. 1991*b* Atomization and dispersion of quasimonodisperse electrostatic sprays systems. In Proc. Fifth Intl Conf. on Liquid Atomization and Spray Systems (ed. H. Semerjian). NTIS Special Publication 813, pp. 805–812.

GOMEZ, A. & TANG, K. 1993 Charged droplet fission in electrostatic sprays. *Phys. Fluids* (to appear).

HAYATI, I., BAILEY, A.. I. & TADROS, TH. F. 1986 Mechanism of stable jet formation in electrohydrodynamic atomization. *Nature*, **319**, 41–43.

HAYATI, I., BAILEY, A. I. & TADROS, TH. F. 1987*a* Investigations into the mechanism of electrohydrodynamic spraying of liquids, I. *J. Colloid Interface Sci.* **117**, 205–221.

HAYATI, I., BAILEY, A. I. & TADROS, TH. F. 1987*b* Investigations into the mechanism of electrohydrodynamic spraying of liquids, II. *J. Colloid Interface Sci.* **117**, 222–230.

JONES, A. R. & THONG, K. C. 1971 The production of charged monodisperse fuel droplets by electrostatic dispersion., *J. Phys.* D: *Appl. Phys.* **4**, 1159.

KIDD, P. W. 1968 Parametric studies with a single-needle colloidal thruster. *J. Spacecraft* **5**, 1034–1039.

MOORE, W. J. 1972 *Physical Chemistry*. Prentice Hall.

PFEIFER, R. J. & HENDRICKS, C. D. 1968 Parametric studies of electrohydrodynamic spraying. *AIAA J.* **6**, 496–502.

RIDDICK, J. A., BUNGER, W. B. & SAKANO, T. 1986 *Organic solvents: Physical Properties and Method of Purification*, 3rd edn. Wiley-Interscience.

ROSELL-LLOMPART, J. & FERNÁNDEZ DE LA MORA, J. 1994 Generation of monodisperse droplets 0.3 to 4 μm in diameter from electrified cone jets. *J. Aerosol Sci.* (submitted).

SMITH, D. P. H. 1986 The electrohydrodynamic atomization of liquids. *IEEE Trans. Ind. Applics* **IA-22**, 527–535.

SMITH, R. D., LOO, J. A., OGORZALEK, R. R., BUSMAN, M. & USDETH, H. R. 1991 Principles and practice of electrospray ionization mass spectrometry for large polypeptides and proteins. *Mass Spectrom. Rev.* **10**, 359–451.

TANG, L. & KEBARLE, P. 1991 Effect of the conductivity of the electrosprayed solution on the electrospray current. Factors determining analyte sensitivity in electrospray mass spectrometry. *Anal. Chem.* **63**, 2709–2715.

TAYLOR, G. I. 1964 Disintegration of water drops in an electric field. *Proc. R. Soc. Lond.* A **280**, 383–397. (See also *The Complete Works of G. I. Taylor* (ed. G. K. Batchelor), Vol. IV; Nos. 9, 39, 40, 41, 42, and 47, Cambridge University Press.)

WEAST, R. C. (ED.) 1985 *Handbook of Chemistry and Physics*, 65th edn. Chemical Rubber Company.

ZELENY, J. 1914 The electrical discharge from liquid points and a hydrostatic method of measuring the electric intensity at their surface. *Phys. Rev.* **3**, 69–91.

ZELENY, J. 1915 On the conditions of instability of liquid drops, with applications to the electrical discharge from liquid points. *Proc. Camb. Phil. Soc.* **18**, 71–93.

ZELENY, J. 1917 Instability of electrified liquid surfaces. *Phys. Rev.* **10**, 1–6.